Jensen, K., Shiels, C. & Freemont, P.S. (2001) PML protein isoforms and the RBCC/TRIM motif. *Oncogene* **20**, 7223–7233.

Joazeiro, C.A. & Weissman, A.M. (2000) RING finger proteins: mediators of ubiquitin ligase activity. *Cell* **102**, 549–552.

Johnston, J.A. & Madura, K. (2004) Rings, chains and ladders: ubiquitin goes to work in the neuron. *Prog Neurobiol* **73**, 227–257.

Kostova, Z. & Wolf, D.H. (2003) For whom the bell tolls: protein quality control of the endoplasmic reticulum and the ubiquitin–proteasome connection. *EMBO J.* **22**, 2309–2317.

Lenk, U., Yu, H., Walter, J., Gelman, M.S., Hartmann, E., Kopito, R.R. & Sommer, T. (2002) A role for mammalian Ubc6 homologues in ER-associated protein degradation. *J. Cell Sci.* **115**, 3007–3014.

Lerner, M., Corcoran, M., Cepeda, D., Nielsen, M.L., Zubarev, R., Ponten, F., Uhlen, M., Hober, S., Grander, D. & Sangfelt, O. (2007) The RBCC gene RFP2 (Leu5) encodes a novel transmembrane E3 ubiquitin ligase involved in ERAD. *Mol. Biol. Cell* **18**, 1670–1682.

Mizugishi, K., Aruga, J., Nakata, K. & Mikoshiba, K. (2001) Molecular properties of Zic proteins as transcriptional regulators and their relationship to GLI proteins. *J. Biol. Chem.* **276**, 2180–2188.

Mizugishi, K., Hatayama, M., Tohmonda, T., Ogawa, M., Inoue, T., Mikoshiba, K. & Aruga, J. (2004) Myogenic repressor I-mfa interferes with the function of Zic family proteins. *Biochem. Biophys. Res. Commun.* **320**, 233–240.

Moriyoshi, K., Iijima, K., Fujii, H., Ito, H., Cho, Y. & Nakanishi, S. (2004) Seven in absentia homolog 1A mediates ubiquitination and degradation of group 1 metabotropic glutamate receptors. *Proc. Natl. Acad. Sci. USA* **101**, 8614–8619.

Munoz-Alonso, M.J., Guillemain, G., Kassis, N., Girard, J., Burnol, A.F. & Leturque, A. (2000) A novel cytosolic dual specificity phosphatase, interacting with glucokinase, increases glucose phosphorylation rate. *J. Biol. Chem.* **275**, 32406–32412.

Nagai, T., Aruga, J., Minowa, O., Sugimoto, T., Ohno, Y., Noda, T. & Mikoshiba, K. (2000) Zic2 regulates the kinetics of neurulation. *Proc. Natl. Acad. Sci. USA* **97**, 1618–1623.

Nagai, T., Aruga, J., Takada, S., Gunther, T., Sporle, R., Schughart, K. & Mikoshiba, K. (1997) The expression of the mouse Zic1, Zic2, and Zic3 gene suggests an essential role for Zic genes in body pattern formation. *Dev Biol.* **182**, 299–313.

Nakagawa, Y., Kaneko, T., Ogura, T., Suzuki, T., Torii, M., Kaibuchi, K., Arai, K., Nakamura, S. & Nakafuku, M. (1996) Roles of cell-autonomous mechanisms for differential expression of region-specific transcription factors in neuroepithelial cells. *Development* **122**, 2449–2464.

Pickart, C.M. (2001) Mechanisms underlying ubiquitination. *Annu. Rev. Biochem.* **70**, 503–533.

Ravid, T., Kreft, S.G. & Hochstrasser, M. (2006) Membrane and soluble substrates of the Doa10 ubiquitin ligase are degraded by distinct pathways. *EMBO J.* **25**, 533–543.

Reymond, A., Meroni, G., Fantozzi, A., Merla, G., Cairo, S., Luzi, L., Riganelli, D., Zanaria, E., Messali, S., Cainarca, S., Guffanti, A., Minucci, S., Pelicci, P.G. & Ballabio, A. (2001) The tripartite motif family identifies cell compartments. *EMBO J.* **20**, 2140–2151.

Rost, B., Fariselli, P. & Casadio, R. (1996) Topology prediction for helical transmembrane proteins at 86% accuracy. *Protein Sci.* **5**, 1704–1718.

Sommer, T. & Jentsch, S. (1993) A protein translocation defect linked to ubiquitin conjugation at the endoplasmic reticulum. *Nature* **365**, 176–179.

Strausberg, R.L., Feingold, E.A., Grouse, L.H., *et al.* (2002) Generation and initial analysis of more than 15 000 full-length human and mouse cDNA sequences. *Proc. Natl. Acad. Sci. USA* **99**, 16899–16903.

Swanson, R., Locher, M. & Hochstrasser, M. (2001) A conserved ubiquitin ligase of the nuclear envelope/endoplasmic reticulum that functions in both ER-associated and Matα2 repressor degradation. *Genes Dev.* **15**, 2660–2674.

Turner, D.L. & Weintraub, H. (1994) Expression of achaete-scute homolog 3 in *Xenopus* embryos converts ectodermal cells to a neural fate. *Genes Dev.* **8**, 1434–1447.

Yao, I., Takagi, H., Ageta, H., *et al.* (2007) SCRAPPER-dependent ubiquitination of active zone protein RIM1 regulates synaptic vesicle release. *Cell* **130**, 943–957.

Younger, J.M., Chen, L., Ren, H.Y., Rosser, M.F., Turnbull, E.L., Fan, C.Y., Patterson, C. & Cyr, D.M. (2006) Sequential quality-control checkpoints triage misfolded cystic fibrosis transmembrane conductance regulator. *Cell* **126**, 571–582.

Received: 19 September 2007
Accepted: 10 January 2008

Author Query Form

Journal: Genes to Cells

Article: gtc_1169.fm

Dear Author,

During the copy-editing of your paper, the following queries arose. Please respond to these by marking up your proofs with the necessary changes/additions. Please write your answers on the query sheet if there is insufficient space on the page proofs. Please write clearly and follow the conventions shown on the attached corrections sheet. If returning the proof by fax do not write too close to the paper's edge. Please remember that illegible mark-ups may delay publication.

Many thanks for your assistance.

No.	Query	Remarks
1	Author: Please expand the authors name.	
2	Author: Please confirm the locations of manufacturers that are inserted.	
3	Author: All gene names should be in italics and proteins should be in roman. Please check.	

The EMBO Journal (2008) 27, 2432–2443 | © 2008 European Molecular Biology Organization | All Rights Reserved 0261-4189/08
www.embojournal.org

THE EMBO JOURNAL

Phosphorylation of 4E-BP by LRRK2 affects the maintenance of dopaminergic neurons in *Drosophila*

Yuzuru Imai[1,*], Stephan Gehrke[2,3], Hua-Qin Wang[4], Ryosuke Takahashi[4], Kazuko Hasegawa[5], Etsuro Oota[6] and Bingwei Lu[2,3,*]

[1]Institute of Development, Aging and Cancer, Tohoku University, Sendai, Japan, [2]Department of Pathology, Stanford University School of Medicine, Palo Alto, CA, USA, [3]GRECC/VAPAHCS, Palo Alto, CA, USA, [4]Department of Neurology, Kyoto University Graduate School of Medicine, Kyoto, Japan, [5]Department of Neurology, Sagamihara National Hospital, National Hospital Organization, Sagamihara, Japan and [6]Division of Clinical Immunology, Kitasato University Graduate School of Medical Science, Sagamihara, Japan

Dominant mutations in leucine-rich repeat kinase 2 (LRRK2) are the most frequent molecular lesions so far found in Parkinson's disease (PD), an age-dependent neurodegenerative disorder affecting dopaminergic (DA) neuron. The molecular mechanisms by which mutations in LRRK2 cause DA degeneration in PD are not understood. Here, we show that both human LRRK2 and the *Drosophila* orthologue of LRRK2 phosphorylate eukaryotic initiation factor 4E (eIF4E)-binding protein (4E-BP), a negative regulator of eIF4E-mediated protein translation and a key mediator of various stress responses. Although modulation of the eIF4E/4E-BP pathway by LRRK2 stimulates eIF4E-mediated protein translation both *in vivo* and *in vitro*, it attenuates resistance to oxidative stress and survival of DA neuron in *Drosophila*. Our results suggest that chronic inactivation of 4E-BP by LRRK2 with pathogenic mutations deregulates protein translation, eventually resulting in age-dependent loss of DA neurons.
The EMBO Journal (2008) **27**, 2432–2443. doi:10.1038/emboj.2008.163; Published online 14 August 2008
Subject Categories: neuroscience; molecular biology of disease
Keywords: 4E-BP; dopaminergic neurodegeneration; LRRK2; Parkinson's disease; protein translation

Introduction

Parkinson's disease (PD) is a neurodegenerative disease that affects the maintenance of dopaminergic (DA) neurons. PD prevalence is estimated at ~1% among people over the age of 65 years and is increased to 5% for people aged 85 years and older. Most PD cases are sporadic, with oxidative stress being one prominent pathological feature (Jenner, 2003). A small percentage of PD cases are inherited in a Mendelian manner, and several disease-causing genes have been identified (Moore *et al*, 2005). Although most of the familial cases are of early onset, mutations in *leucine-rich repeat kinase 2* (*LRRK2*) cause an autosomal-dominant form of familial PD late in life (Paisan-Ruiz *et al*, 2004; Zimprich *et al*, 2004). *LRRK2* encodes a large protein with multiple domains, including GTPase and kinase domains. *LRRK2*-associated familial PD is largely indistinguishable from the more common sporadic PD in clinical and pathological aspects. Among the known familial PD genes, *LRRK2* is most frequently mutated in sporadic cases, suggesting a general involvement of *LRRK2* in PD pathogenesis (Taylor *et al*, 2006). So far, amino-acid substitutions associated with familial PD have been identified within the multiple domains (Mata *et al*, 2006). Some pathogenic mutations in the kinase domain, such as G2019S and I2020T, were shown to cause moderately enhanced kinase activity *in vitro* (West *et al*, 2005; Gloeckner *et al*, 2006). It is not clear whether mutations in other domains (e.g., R1441G and Y1699C) also affect kinase activity. The pathogenic function of LRRK2 mutations and the biochemical pathways involved are unknown. Key to addressing these important questions is the identification of the physiological substrate(s) of LRRK2.

Translational control is critical for early development of most metazoans and for cell survival under various stress (Holcik and Sonenberg, 2005). It allows an organism to quickly respond to physiological or environmental cues by controlling the expression of proteins from existing mRNAs. Although translation can be regulated at multiple steps, control of translation initiation represents a primary regulatory mechanism. The eukaryotic initiation factor 4E (eIF4E) subunit mediates the binding of eIF4F to the 5′ m^7GpppX cap structure of mRNAs (Sonenberg *et al*, 1979; Gingras *et al*, 1999b). The activity of eIF4E is inhibited by eIF4E-binding protein (4E-BP), which sequesters eIF4E from the eIF4F complex (Gingras *et al*, 1999b; Richter and Sonenberg, 2005). *In vivo*, 4E-BP has an important function for survival under starvation stress, oxidative stress and unfolded protein stress, suggesting that control of translation initiation is closely linked to stress and lifespan (Teleman *et al*, 2005; Tettweiler *et al*, 2005; Yamaguchi *et al*, 2008). 4E-BP is regulated by phosphorylation. One pathway known to influence 4E-BP phosphorylation is the target of rapamycin (TOR) pathway, which integrates nutrient availability, growth factors and cellular energy status to control cell growth. Phosphorylation of 4E-BP causes its release from the eIF4E and relieves its inhibitory effect on translation (Gingras *et al*, 2001; Inoki *et al*, 2005). At least six phosphorylation sites have been identified in human 4E-BP1 (h4E-BP1), including

*Corresponding authors. Y Imai, Institute of Development, Aging and Cancer, Tohoku University, 4-1 Seiryo-Machi, Aoba-Ku, Sendai, Miyagi 980-8575, Japan. Tel.: +81 22 717 8490; Fax: +81 22 717 8490; E-mail: yimai@idac.tohoku.ac.jp or B Lu, GRECC/VAPAHCS, 3801 Miranda Ave, Bldg. 100, Palo Alto, CA 94304, USA. Tel.: +650 849 0373; Fax: +650 852 3440; E-mail: bingwei@stanford.edu

Received: 31 March 2008; accepted: 25 July 2008; published online: 14 August 2008

T37, T46, S65, T70, S83 and S112 (Fadden *et al*, 1997; Heesom *et al*, 1998). A sequential phosphorylation of 4E-BP1 in the order of T37/T46>T70>S65 has been proposed (Gingras *et al*, 1999a, 2001). Although the regulatory mechanisms involved in 4E-BP phosphorylation are not fully understood, it appears that a combination of perhaps all phosphorylation events is required to dissociate 4E-BP from eIF4E (Gingras *et al*, 2001).

Here, we show that LRRK2 exerts an effect as a regulator of protein translation by phosphorylating 4E-BP at the T37/T46 sites *in vitro* and *in vivo*. These phosphorylation events appear to be functionally important for the *in vivo* pathogenic effects of the mutant *Drosophila* orthologue of LRRK2 (dLRRK) on stress sensitivity and DA neuron survival. Our results suggest a novel molecular mechanism linking deregulated protein translation to stress sensitivity and neurodegeneration in PD.

Results

dLRRK regulates DA neuron function and maintenance

To understand the biological function and pathogenic function of human LRRK2 (hLRRK2), we have used *Drosophila* as a model system. *Drosophila*, which possesses a dopaminergic system regulating locomotor behaviour and has a short lifespan, is particularly suitable for modelling the late-onset PD caused by LRRK2 mutations. A single orthologue of *LRRK2* (referred to as *dLRRK* hereafter) was identified in the *Drosophila* genome. We cloned full-length *dLRRK* cDNA by RT–PCR. It encodes a 2445 amino-acid protein containing the various domains found in hLRRK2. Critical residues disrupted in familial PD are conserved between hLRRK2 and dLRRK (Figure 1A).

To study the biological function of dLRRK, we analysed its gain-of-function (GOF) and loss-of-function (LOF) effects. For GOF analysis, we generated transgenic (Tg) flies expressing wild-type (WT) dLRRK or mutant dLRRK carrying point mutations found in human PD patients (Figure 1B and Supplementary Figure 1). The DA neuron-specific *tyrosine hydroxylase* (*TH*)- and *dopa decarboxylase* (*Ddc*)-*Gal4* drivers, pan-neuronal *elav-Gal4* driver or the ubiquitous *daughterless* (*Da*)-*Gal4* driver were used to direct transgene expression. For LOF analysis, we obtained one P-element insertion line, in which the expression of full-length dLRRK protein is disrupted, as indicated by the lack of detectable full-length dLRRK protein expression (Figure 1B). In addition, there was no detectable expression of a truncated dLRRK (data not shown). By RT–PCR analysis, we determined that the expression levels of the two genes immediately flanking *dLRRK* were not affected in this *dLRRK* (−/−) mutant (Supplementary Figure 2). Mutant animals are viable, but have decreased fertility in females. In addition, malformed abdomen is often observed in females (Figure 1C), especially when nutritional status is compromised at the larval stage. Because mutants with this phenotype show higher sensitivity to various stress and have shortened lifespan, we excluded them in subsequent analyses.

To test whether dLRRK regulates the function and maintenance of DA neurons, we performed immunohistochemical and neurochemical analyses in *Drosophila*. Immunohistochemical analysis using an anti-dLRRK antibody showed that endogenous dLRRK protein expression is fairly ubiquitous in the fly brain (Supplementary Figure 1B and C). Double labelling with TH showed that it is expressed in DA neurons (Supplementary Figure 1M and N). In Tg animals, we estimated that exogenous WT and mutant dLRRK were expressed at 1.5- to 2.6-fold of endogenous level in TH+ neurons (Supplementary Figure 1M). At the cellular level, endogenous dLRRK was localized in a punctate pattern in the cytoplasmic part of the cell bodies and neurites (Supplementary Figure 1L). Transgenic WT and mutant dLRRK proteins derived from the transgenes were also localized to vesicular structures that co-stain with endosomal markers and partially overlap with synaptic vesicle markers (Supplementary Figure 1H–K and O–V).

In Tg flies expressing PD-related mutant dLRRK, brain dopamine content was significantly reduced compared with dLRRK WT Tg or control flies (Figure 1D, left). Conversely, dopamine content was elevated in *dLRRK* (−/−) flies, suggesting that dLRRK negatively regulates steady-state dopamine levels (Figure 1D, right). We tested whether this difference in DA content might reflect differential maintenance of DA neurons. In young flies (10-day-old), no difference in DA neuron number was observed when compared with a normal control (Supplementary Figure 3). In aged flies (60-day-old), however, animals expressing pathogenic dLRRK showed a significant reduction of DA neurons in the protocerebral posterior lateral (PPL) 1 and protocerebral posterior medial (PPM) 1 and 2 clusters (Figure 1E). Expression of a kinase-dead form (3KD) of dLRRK or WT dLRRK had no significant effect on DA neuron number (Figure 1E). In both young and aged *dLRRK* (−/−) flies, DA neurons appeared healthy and well maintained (Figure 1E and Supplementary Figure 3). The increase of brain dopamine level in *dLRRK* (−/−) flies is thus likely due to changes of dopamine transmission, storage or metabolism, but not to a change of TH+ neuron number.

Transgenic animals were morphologically normal when dLRRK was ubiquitously expressed. No gross brain degeneration other than DA neuron loss was observed when dLRRK was pan-neuronally expressed, and no neurodegeneration was observed when dLRRK was expressed in specific neuronal types (Supplementary Figure 4 and data not shown), indicating that the toxicity of mutant dLRRK is relatively specific to DA neurons.

Altered dLRRK expression affects organismal sensitivity to oxidative stress

We further analysed animals with altered dLRRK activities to gain insight into the effect of dLRRK on DA neuron maintenance. Oxidative stress is suspected as one of the major causes of DA neuron degeneration in PD. We tested whether dLRRK Tg flies manifest altered response to oxidative stress. Compared with the controls, flies ubiquitously expressing dLRRK Y1383C and I1915T mutants showed significantly higher sensitivity to exogenous ROS inducers paraquat and H_2O_2 (Figure 2A and B). In contrast, *dLRRK* (−/−) or *dLRRK RNAi* animals were significantly more resistant (Figure 2C and D). Animals transheterozygous for *dLRRK* mutant and a chromosomal deficiency that covers *dLRRK* (*Df*/−) were also more resistant to H_2O_2 (Figure 2C and D).

To investigate whether dLRRK is involved in cellular response to endogenous oxidative stress, we examined untreated flies for the extent of oxidative damage as measured

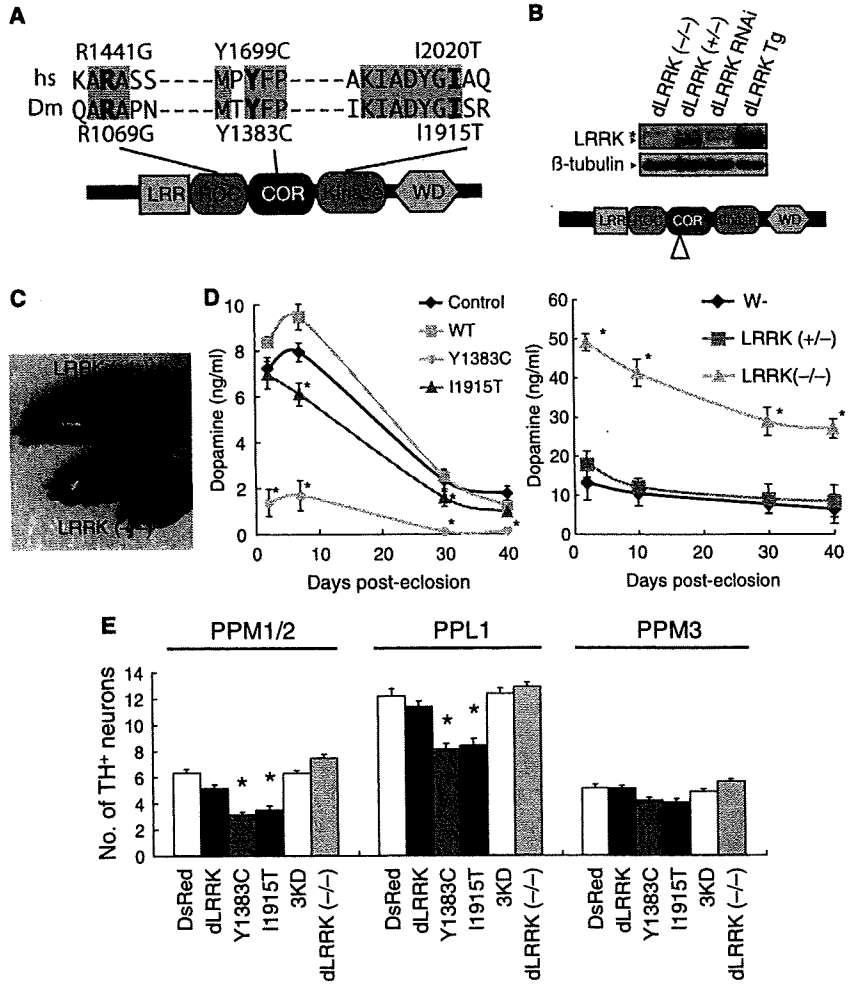

Figure 1 dLRRK regulates function and maintenance of DA neuron. (**A**) A schematic of dLRRK and hLRRK2 domain structures. (**B**) Western blot analysis showing loss of dLRRK protein expression in *dLRRK*(−/−). Brain tissues of 3-day-old adult flies were analysed using anti-dLRRK antibody, which recognizes the N-terminal part of dLRRK. Diagram indicates the location of P-element insertion. (**C**) A phenotype of malformed abdomen observed with incomplete penetrance in *dLRRK*(−/−) females. *dLRRK*(+/−) female shows a normal phenotype. (**D**) Fly heads of dLRRK Tg driven by *Ddc-Gal4* (left) or *dLRRK* mutant animals (right) were used to prepare tissue extracts for dopamine measurement. *Ddc-Gal4*/+ and w^- serves as controls for Tg and *dLRRK* mutant, respectively. The values represent means ± s.e. from five male fly heads in three independent measurements (Asterisk in left and right panels, $P<0.01$ and $P<0.001$, respectively). (**E**) Quantification of TH+ DA neuron number in the PPM 1 and 2, PPL1 and PPM3 clusters in 60-day-old males of the indicated Tg animals driven by *TH-Gal4*. PPM1 and PPM2 cluster neurons were counted together. Data were shown as means ± s.d. (*$P<0.01$ versus *TH-Gal4>DsRed* control, $n=12$ for *dLRRK*(−/−); $n=10$ for the others).

by 4-hydroxy-2-nonenal (4-HNE) immunostaining of lipid peroxidation. An age-dependent increase of 4-HNE level in DA neurons was evident in control flies (Figure 2E and F). In age-matched *dLRRK*(−/−) flies, 4-HNE level was significantly reduced (Figure 2E and F). In contrast, dLRRK Tg animals showed significantly increased 4-HNE levels (Figure 2E and F), with mutant dLRRK showing stronger effect than WT dLRRK. Changes of 4-HNE levels in *dLRRK*(−/−) and Tg animals were confirmed by dot blot analysis of 4-HNE adducts (Supplementary Figure 5A). We also used 2,7-dichlorofluorescein diacetate staining, which is an indicator of hydroxyl-free radical levels, to analyse *dLRRK*(−/−) and Tg flies. Hydroxyl-free radical levels were significantly reduced in *dLRRK* (−/−) and *dLRRK*(*Df*/−) flies, whereas an increase was observed in dLRRK Tg flies (Supplementary Figure 5B). These results suggest a physiological function of dLRRK in handling oxidative stress and a pathological function of heightened oxidative stress in mediating the toxicity of mutant LRRK2.

dLRRK genetically interacts with genes in the TSC/Rheb/TOR/4E-BP pathway

As our previous studies implicated altered PTEN/PI3K/Akt signalling in fly PD models (Yang *et al*, 2005), we tested possible genetic interaction of *dLRRK* with this pathway. *dLRRK* exhibited strong interaction with the TSC/Rheb/TOR/4E-BP pathway, a downstream branch of the PTEN/PI3K/Akt signalling network that regulates cell growth and cell size through protein synthesis. For instance, inhibition of TOR signalling through the co-overexpression of TSC1 and TSC2 inhibited cell growth in the fly eye (Gao and Pan, 2001; Potter *et al*, 2001). This was enhanced by the loss of *dLRRK*

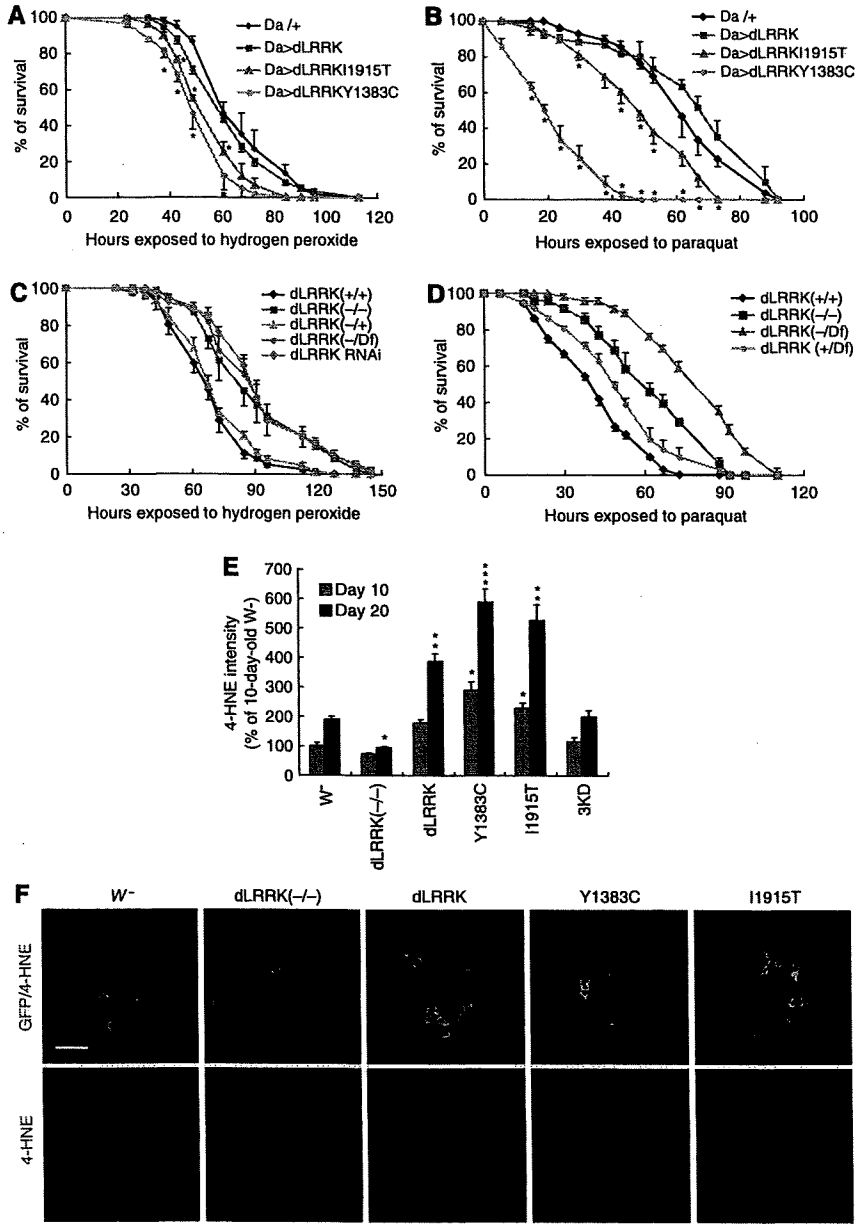

Figure 2 dLRRK regulates stress resistance. (**A**) Response of dLRRK Tg flies to H_2O_2 treatment. Error bars show s.d. from four repeated experiments. $^*P<0.05$, Y1383C and I1915T versus *Da-Gal4/+* control (all, $n=60$). (**B**) Response of dLRRK Tg to paraquat treatment. Error bars show s.d. from three repeated experiments. $^*P<0.05$, Y1383C ($n=48$) and I1915T ($n=48$) versus *Da-Gal4/+* ($n=84$). (**C**) Response of *dLRRK*(−/−) ($n=85$), *dLRRK*(*Df*/−) ($n=84$) and *dLRRK RNAi* flies ($n=85$) to H_2O_2 treatment. Error bars show s.d. from three repeated experiments. $P<0.01$ versus *dLRRK*(+/+) control ($n=89$) for all values at 61–128 h. *Df*/+ and *dLRRK*(+/+) serve as controls. Transgene and RNAi expressions were directed by *Da-Gal4* in A–C. (**D**) Response of *dLRRK*(−/−) ($n=48$) and *dLRRK*(*Df*/−) flies ($n=46$) to paraquat treatment. Error bars show s.d. from three repeated experiments. $P<0.001$, versus *dLRRK*(+/+) ($n=72$) for all values at 24–73 h. (**E**) Statistical analysis of 4-HNE levels among the indicated genotypes crossed with a *TH-Gal4>UAS-GFP* line at 10- and 20-day of age raised at 29°C. 4-HNE levels from 25–30 TH+ neurons in the PPL1 clusters were quantified after normalization with GFP signal. $^*P<0.05$; $^{**}P<0.01$; $^{***}P<0.001$ versus w^- × *TH-Gal4>GFP* cross (w^-). (**F**) Representative images of PPL1 clusters of the indicated genotypes double-stained for GFP (green) and 4-HNE (red). Scale bar = 20 μm.

(Supplementary Figure 6C), although loss of *dLRRK* in an otherwise WT background had no effect (Supplementary Figure 6A and F). Conversely, stimulation of TOR signalling by Rheb overexpression enhanced cell growth (Saucedo *et al*, 2003), which was partially suppressed by the loss of *dLRRK* (Supplementary Figure 6E and G). Overexpression of a constitutively active form of d4E-BP (4E-BP(LL)), which has stronger affinity for eIF4E (Miron *et al*, 2001), caused a mild reduction of eye size (Supplementary Figure 6H). This effect was significantly enhanced by the loss of *dLRRK* (Supplementary Figure 6I). As the numbers of ommatidia per fly eye and rhabdomeres per ommatidium were not

changed (Supplementary Figure 6J and K), the reduction of eye size was mostly due to a reduction of cell size, a measure of cell growth. The genetic interaction between *dLRRK* and *4E-BP* was also evident in other tissues. Overexpression of 4E-BP(LL) in wing imaginal discs with the *MS1096-Gal4* driver resulted in a moderate reduction of wing size (Miron *et al*, 2001), which was enhanced by the loss of *dLRRK* (Supplementary Figure 6L and N). The effect of removal of *dLRRK* on TSC1, TSC2 and Rheb overexpression was recapitulated by dLRRK knockdown and was rescued by the introduction of dLRRK WT but not 3KD transgenes (Supplementary Figure 7). These results suggest that dLRRK positively regulates cell growth through interaction with the TSC/Rheb/TOR/4E-BP pathway of protein translational control.

LRRK2 phosphorylates 4E-BP

We then sought to investigate the molecular mechanism underlying the effect of dLRRK on protein translation. To study its biochemical function, we purified dLRRK from transfected 293T cells by immunoprecipitation (IP). dLRRK purified this way possessed kinase activity, as shown by autophosphorylation (Figure 3A, upper panel in lane 2 compared with lane 1). As a control, we similarly purified a mutant dLRRK containing three point mutations (3KD), including the K1781 mutation predicted to disrupt ATP-binding (Greggio *et al*, 2006). The 3KD mutant exhibited no kinase activity, suggesting that the activity detected above was derived from dLRRK rather than some associated kinases in the IP complex (Figure 3A, lane 3). We also purified dLRRK containing PD-associated point mutations. The kinase activity of dLRRK containing the I1915T mutation was notably higher than WT dLRRK (Figure 3B, lane 4 compared with lane 2).

Having obtained active dLRRK kinase, we next searched for its substrate(s). On the basis of the genetic interaction data, we tested candidate proteins in the TSC/Rheb/TOR/4E-BP signalling pathway. Robust phosphorylation of d4E-BP by dLRRK was detected (Figure 3A, lane 2). The activities of WT and I1915T mutant dLRRK towards d4E-BP correlated with their autophosphorylation activity (Figure 3B, lanes 2–4). eIF4E, the binding partner of 4E-BP and itself a phospho protein, was not phosphorylated by dLRRK (Supplementary Figure 8), supporting the specificity of dLRRK action towards d4E-BP. The situation holds true for the human proteins, with purified hLRRK2 robustly phosphorylating h4E-BP1 and the I2020T mutant possessing a higher activity (Figure 3C, lane 3 compared with lane 2).

To precisely map the phosphorylation site(s) in h4E-BP1, we made a series of Ser/Thr to Ala substitutions in h4E-BP1 and tested their effects on phosphorylation by hLRRK2 *in vitro*. Mutating T37/T46 and S65 reduced the amount of P^{32} incorporation, whereas mutating T70 and S83 had minimal effect (Figure 3D, lanes 7 and 9 compared with lanes 10 and 12). Combining T37/T46A and S65A mutations further reduced P^{32} incorporation (Figure 3D, lane 3). Addition of a T70A mutation into the T37/T46/S65A triple mutant background had no further effect (Figure 3D, lane 4 compared with lane 3). Western blot analysis of *in vitro*-phosphorylated h4E-BP1 with phospho-specific antibodies showed that the T37/T46 and S65 sites were directly phosphorylated by hLRRK2 (Supplementary Figure 9). Similarly, T37/T46A mutations in *Drosophila* 4E-BP reduced its phosphorylation by dLRRK (Figure 3E, lane 3 compared with lane 2). These *in vitro* results suggest that T37/T46 and S65 in 4E-BP represent major LRRK2 target sites.

To verify the *in vitro* phosphorylation result, we examined the effect of overexpression or knockdown of hLRRK2 on h4E-BP1 phosphorylation. A clear increase of h4E-BP1 phosphorylation at T37/T46 was observed in cells transfected with WT or mutant hLRRK2 (I2020T) (Figure 3F, lanes 2 and 3 compared with lane 1). In contrast, p-T37/T46 level was reduced in cells transfected with hLRRK2 siRNA, which effectively knocked down hLRRK2 expression (Figure 3G), whereas a control siRNA had no effect. As mTOR is known to affect 4E-BP phosphorylation, we tested whether hLRRK2 might exert an effect through mTOR. No change in mTOR phosphorylation or protein level was observed when hLRRK2 activity was altered (Supplementary Figure 10). Thus, the

Figure 3 dLRRK and hLRRK2 phosphorylate 4E-BP. (**A–C**) *In vitro* kinase assays using dLRRK and d4E-BP (A, B) or hLRRK2 and h4E-BP1 (C) as kinase–substrate pairs. Mock immunoprecipitate (IP) serves as control. Autoradiography (P^{32}), western blot (WB) and Coomassie brilliant blue (CBB) staining of the gels are shown. The asterisk in C marks a putative truncated form of hLRRK2 often observed in the IP fraction. (**D, E**) *In vitro* kinase assay using hLRRK2 (D) or dLRRK (E) as the kinase and a series of wild-type (WT) and mutant h4E-BP1 (D) or d4E-BP (E) as substrates. Mock IP serves as kinase control. CBB: protein loading control. The Ser or Thr residues mutated to Ala are indicated. (**F, G**) Western blot analysis showing effects of altered hLRRK2 activities on endogenous h4E-BP1 phosphorylation in 293T cells, which were starved for 24 h and then stimulated with 1 μg/ml insulin for 30 min. (F) Overexpression of WT and I2020T mutant hLRRK2 increased h4E-BP1 phosphorylation at T37/T46 and T70. Mock transfection serves as control. (G) Knockdown of hLRRK2 by RNAi reduced h4E-BP1 phosphorylation at T37/T46 and T70. Control: a non-targeting siRNA. Graphs show relative levels of p-T37/T46, p-T70 and p-S65 after normalization with total h4E-BP1 level. Values represent means ± s.d. from three experiments (*$P<0.05$; **$P<0.01$ in Bonferroni/Dunn test). (**H**) dLRRK influences d4E-BP phosphorylation *in vivo*. d4E-BP protein was immunoprecipitated with a d4E-BP antibody from fly brain extracts of the indicated genotypes. Immunoprecipitated d4E-BP was detected by western blot with p-T37/T46 (upper) and total d4E-BP (lower) antibodies. Bands corresponding to phosphorylated (β) and non-phosphorylated forms (α) of d4E-BP are indicated in the total d4E-BP western. Graph shows relative level of p-T37/T46 after normalization with total d4E-BP level. Values represent means ± s.d. from three experiments (*$P<0.05$; **$P<0.01$ in Bonferroni/Dunn test). (**I, J**) Immunohistochemical analysis showing that dLRRK promotes d4E-BP phosphorylation. Adult brain TH-positive neurons were co-stained with anti-TH and anti-p-T37/T46 in control *w−* or dLRRK Tg crossed with *TH-Gal4*. Representative images are shown in I. The p-T37/T46 signals were quantified after normalization with TH signals. Values represent means ± s.d. from three independent experiments (*$P<0.05$; **$P<0.01$). (**K**) Western blot analysis showing effects of pathogenic hLRRK2 mutations on h4E-BP1 phosphorylation at T37/T46 sites in serum-starved 293T cells. The graph shows quantification of the relative level of p-T37/T46 after normalization with total h4E-BP1 level. Values represent means ± s.d. from three independent experiments (*$P<0.05$; **$P<0.01$ versus hLRRK2 WT). (**L**) hLRRK2 stimulates protein synthesis *in vitro* in a kinase activity-dependent manner. Immunopurified FLAG-hLRRK2 WT, I2020T and 3KD proteins together with capped *firefly* luciferase mRNA were incubated in rabbit reticulocyte lysate (Promega) for 2.5 h at 30 °C. The activity of luciferase translated in the lysate was measured (graph, means ± s.d. from three independent experiments). *$P<0.05$ versus mock. Western blot and RT–PCR was performed for estimation of protein and mRNA levels in the lysate. PCR without RT (PCR) serves as a negative control for RT–PCR.

T37/T46 sites in h4E-BP1 appeared to be physiological hLRRK2 target sites. Despite the fact that T70 was not directly modified by hLRRK2 *in vitro*, its phosphorylation was affected by alterations of hLRRK2 in the cultured cells (Figure 3F and G). This is consistent with the notion that p-T37/T46 may prime subsequent T70 phosphorylation (Gingras *et al*, 2001) by other kinases. Alternatively, T70 could be a direct target of dLRRK *in vivo*. On the other hand, although S65 was modified by hLRRK2 *in vitro*, its phosphorylation was not affected by hLRRK2 in cultured cells (Figures 3F and G). The S65 site may be more tightly regulated by other kinases or phosphatases *in vivo*.

We sought for further *in vivo* evidence that LRRK2 is a 4E-BP kinase. Western blot and immunostaining of dLRRK Tg and mutant flies showed that phosphorylation of d4E-BP at T37/T46 sites was increased in dLRRK Tg but decreased in *dLRRK*(−/−) flies, supporting the fact that T37/T46 in d4E-BP are *in vivo* dLRRK target sites (Figure 3H–J). Note that, in *dLRRK*(−/−) mutant flies, phosphorylation of d4E-BP at T37/T46 sites was reduced but not abolished, suggesting that there exist other kinase(s) that exert an effect on these sites. Both WT and a pathogenic LRRK2 effectively stimulated the phosphorylation of T37/T46 sites of 4E-BP1 to similar levels upon insulin treatment (Figure 3F). Under starvation (serum-free) condition, however, some pathogenic mutants exhibit higher kinase activity than WT LRRK2 (Figure 3K). These data suggested that LRRK2 interacts with the insulin/IGF signalling pathway to regulate 4E-BP phosphorylation, but

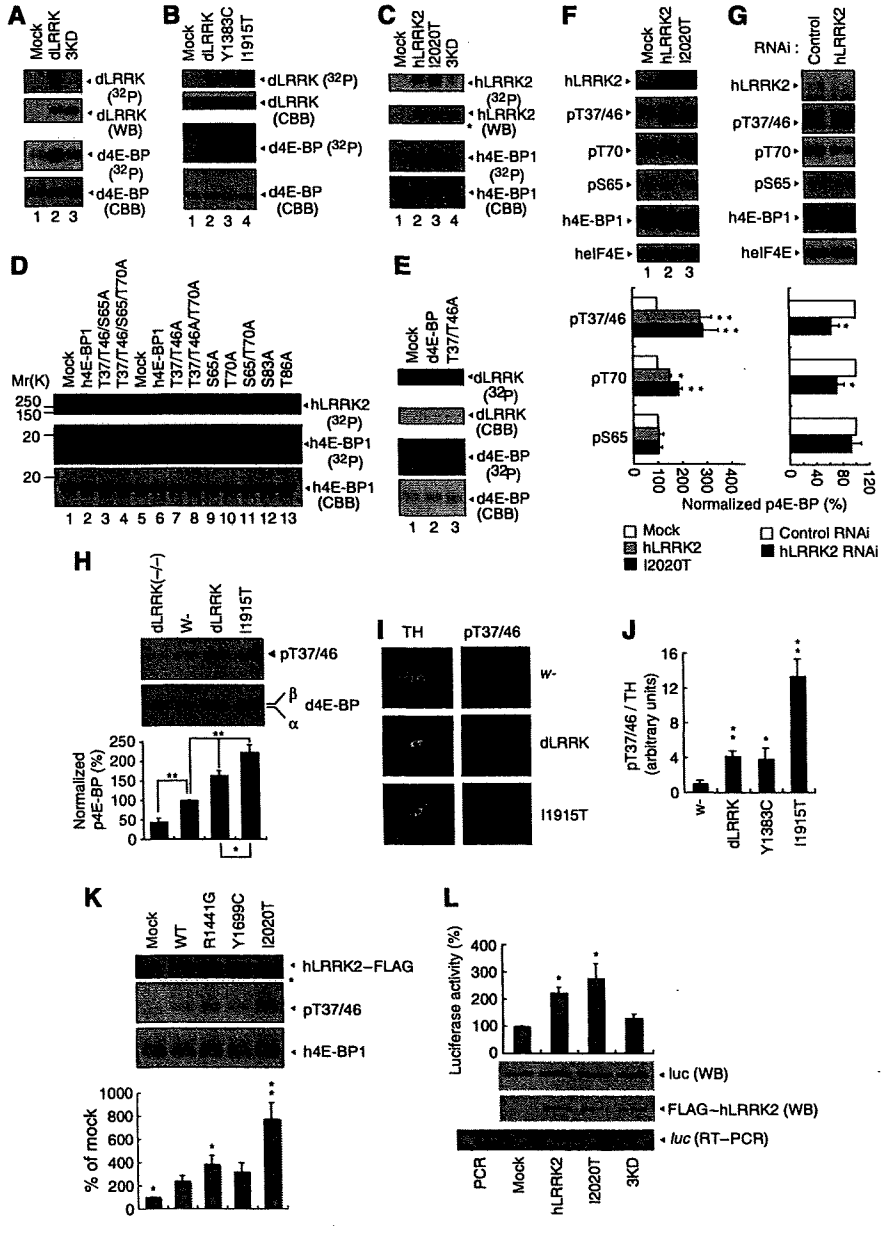

the kinase activity of some pathogenic mutants is not dependent on insulin/IGF stimulation.

The genetic interaction between *LRRK2* and the TSC/Rheb/TOR/4E-BP pathway of growth control and the phosphorylation of 4E-BP by LRRK2 suggest that LRRK2 is a positive regulator of protein translation. Consistent with this notion, direct addition of purified hLRRK2 WT and I2020T proteins to an *in vitro* translation system effectively stimulated the translation of a luciferase reporter mRNA, whereas hLRRK2 3KD had no effect (Figure 3L).

Activities of 4E-BP and eIF4E are important for cellular stress response and DA neuron maintenance

Previous studies revealed a function for d4E-BP in conferring resistance against starvation and oxidative stress (Teleman *et al*, 2005; Tettweiler *et al*, 2005). We asked whether phosphorylation of 4E-BP at T37/T46 residues, which is promoted by dLRRK kinase activity, affects resistance to oxidative stress *in vivo*. For this purpose, we generated Tg flies expressing d4E-BP T37/T46A (TA) mutant protein. Whereas expression of d4E-BP WT restored oxidative stress resistance in *d4E-BP*(−/−), expression of similar levels of d4E-BP TA resulted in higher resistance against oxidative stress (Figure 4A and B, and Supplementary Figure 11). This suggests that complete blockage of 4E-BP T37/T46 phosphorylation and the consequent tighter binding and stronger inhibition of eIF4E lead to higher stress resistance. To test this idea further, we asked whether manipulation of eIF4E is sufficient to alter oxidative stress response. Overexpression of deIF4E significantly sensitized animals to oxidative stress treatments, similar to the effect induced by mutant dLRRK overexpression (Figure 4C). Furthermore, deIF4E Tg animals showed a significant increase of 4-HNE in the absence of stress (Figure 4D), suggesting that excessive eIF4E activity altered endogenous stress response and resulted in more oxidative damages.

Consistent with the above findings, removal of one copy of *deIF4E* in dLRRK I1915T Tg flies increased resistance against oxidative stress (Figure 4E). We further tested whether the co-expression of d4E-BP TA mutant, by inhibiting the release of d4E-BP from deIF4E, rendered dLRRK I1915T flies more resistant to oxidative stress. This was indeed the case (Supplementary Figure 12). We next used 7-methyl GTP (m^7GTP) sepharose-binding assay to biochemically assess the level of 4E-BP-free eIF4E, an indicator of translation efficiency, in the various genetic backgrounds. *In vivo*, eIF4E protein level is fairly constant and both the 4E-BP-bound and 4E-BP-free forms of eIF4E bind to m^7GTP sepharose beads. By measuring the amount of 4E-BP-bound eIF4E, we can get an estimate of 4E-BP-free, active eIF4E. As shown in Figure 4F, in d4E-BP WT Tg animals co-expressing GFP, a significant portion of d4E-BP WT was released from deIF4E under normal conditions; however, under oxidative stress condition, almost all d4E-BP WT was bound to deIF4E (Figure 4F, lanes 1 and 2). The amount of d4E-BP WT released from deIF4E was increased in the presence of dLRRK I1915T under both normal and oxidative stress conditions (Figure 4F, lanes 3 and 4). In contrast, d4E-BP TA was tightly bound to eIF4E in the presence or absence of dLRRK I1915T, and under normal or stress conditions (Figure 4F, lanes 5–8). These results suggested that dLRRK releases the inhibition of eIF4E by 4E-BP, enabling free eIF4E to engage in translation.

We next tested whether d4E-BP and deIF4E influence dLRRK-mediated DA neurodegeneration in the flies. Whereas overexpression of d4E-BP had no effect on DA neuron number in control Tg flies, it partially suppressed the DA neuron loss phenotype seen in dLRRK Tg flies (Figure 5A). Introduction of d4E-BP TA fully protected against DA neuron loss caused by dLRRK I1915T (Figure 5B). Furthermore, introduction of d4E-BP WT rescued DA neuron loss seen in *d4E-BP*(−/−) flies (Figure 5B). Supporting a function for deregulation of the eIF4E/4E-BP pathway in inducing DA neuron loss, overexpression of deIF4E alone caused a reduction of DA neurons; however, in *dLRRK*(−/−) background, this effect of deIF4E was suppressed (Figure 5C). Given that DA neuron loss was observed in aged dLRRK Tg flies, we searched for evidence of motor dysfunction caused by DA degeneration. As shown in Figure 5D, dLRRK I1915T expression caused locomotor dysfunction with age, which was improved by the co-expression of d4E-BP TA (Figure 5D). Taken together, these results indicate that the interaction between dLRRK and the eIF4E/4E-BP pathway is intimately involved in the maintenance of DA neurons.

Discussion

In this study, we used *Drosophila* as a model system to understand the normal physiological function of LRRK2 and how its dysfunction leads to DA neurodegeneration. We provide genetic and biochemical evidence that dLRRK modulates the maintenance of DA neuron by regulating protein synthesis. We demonstrate that LRRK2 primes phosphorylation of 4E-BP and that this event has an important function in mediating the pathogenic effects of mutant dLRRK. These results for the first time link deregulation of the eIF4E/4E-BP pathway of protein translation with DA degeneration in PD.

eIF4E is a key component of the eIF4F complex that initiates cap-dependent protein synthesis. It has long been recognized that a key mechanism regulating eIF4E function is through phosphorylation-induced release of 4E-BP from eIF4E. A number of candidate kinases, including mTOR, have been implicated on the basis of *in vitro* or cell culture studies, but the physiological kinases remain to be identified. We show here that LRRK2 is one of the physiological kinases for 4E-BP. LRRK2 exerts an effect on 4E-BP primarily at the T37/T46 sites. Phosphorylation at T37/T46 by LRRK2 likely facilitates subsequent phosphorylation at T70 and S65 *in vivo* by other kinase or LRRK2 itself. 4E-BP phosphorylation by LRRK2, therefore, could serve as an initiating event in an ordered, multisite phosphorylation process to generate hyperphosphorylated 4E-BP (Figure 6), similar to the phosphorylation of the Alzheimer's disease-associated tau (Nishimura *et al*, 2004). Our results show that LRRK2 is not the only kinase that phosphorylates 4E-BP T37/T46 sites (Figure 3H). Similarly, 4E-BP is unlikely the only substrate of LRRK2. A recent study showed that human LRRK2 phosphorylates moesin (Jaleel *et al*, 2007), the physiological relevance of which remains to be determined.

The role of 4E-BP in regulating eIF4E function has been well established *in vitro*. Recent studies in *Drosophila*, however, have revealed the complexity of the *in vivo* function of 4E-BP. Loss of the only *d4E-BP* gene does not affect cell size

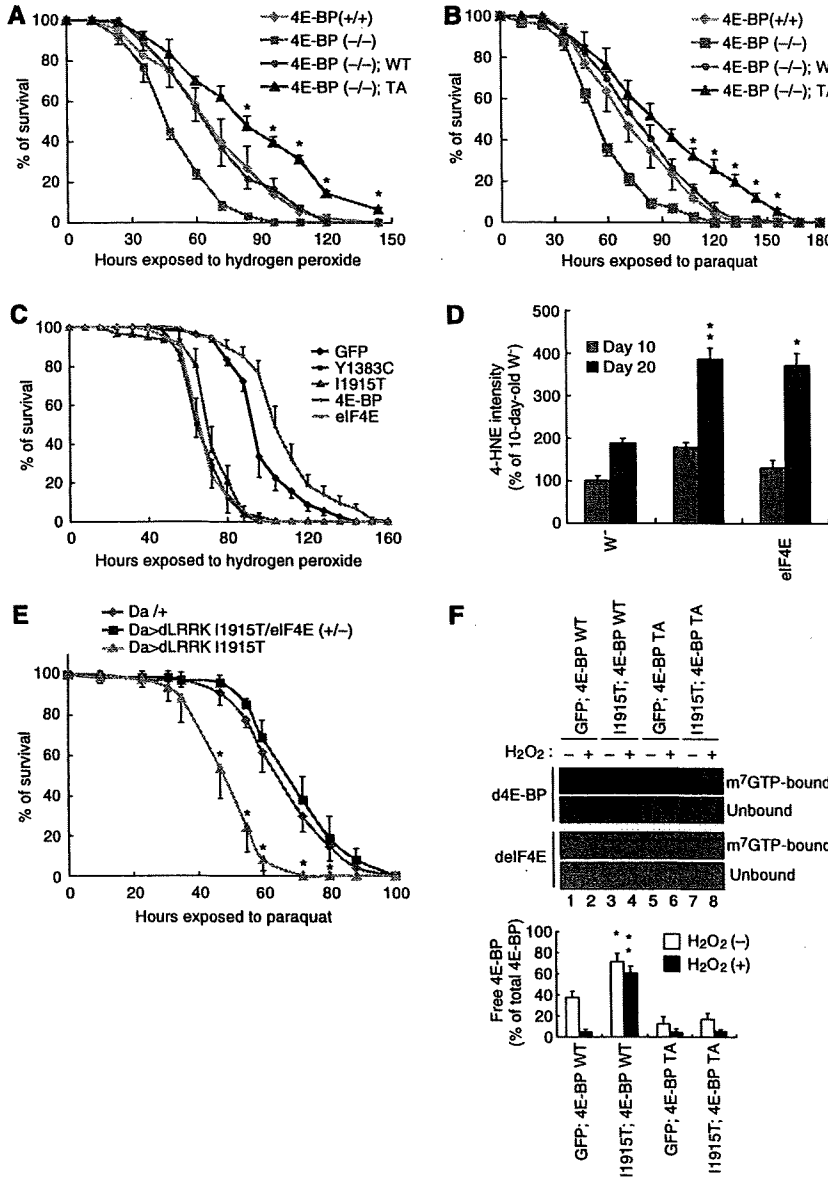

Figure 4 The eIF4E/4E-BP pathway is important for handling oxidative stress. (**A, B**) d4E-BP TA confers H_2O_2 (A) and paraquat (B) resistance. d4E-BP WT or TA mutant were expressed in the *d4E-BP*(−/−) background under *DA-Gal4* control. *$P<0.05$, *d4E-BP*(−/−); *TA* ($n=76$ in A; $n=78$ in B) versus *d4E-BP*(−/−); *WT* ($n=80$ in A; $n=82$ in B). (**C**) Oxidative stress responses of dLRRK, delF4E and d4E-BP Tg flies driven by *Da-Gal4*. delF4E Tg ($n=72$) and the dLRRK Y1383C ($n=72$) or I1915T ($n=85$) Tg were more sensitive to H_2O_2 treatment than the GFP Tg control ($n=90$) ($P<0.01$ for all values at 72–120 h), whereas d4E-BP Tg ($n=90$) was more resistant than the control ($P<0.05$ versus GFP Tg for the values at 72–144 h). (**D**) Overexpression of delF4E or dLRRK increases 4-HNE levels in DA neurons. *TH-Gal4>GFP* was crossed with the indicated genotypes as shown in Figure 2E. Values represent means ± s.d. (*$P<0.05$; **$P<0.01$ versus age-matched *w*−, $n=25$–30). Error bars in (A–D) show s.d. from three repeated experiments. (**E**) Reduction of delF4E function suppresses vulnerability of dLRRK I1915T to oxidative stress induced by paraquat. dLRRK I1915T was expressed in the *delF4E*(+/+) or *delF4E*(+/−) background with *DA-Gal4*. *$P<0.006$, *Da>dLRRK I1915T/delF4E* (+/−) ($n=74$) versus *Da>dLRRK I1915T* ($n=75$). (**F**) m^7GTP pull-down assay showing the effect of dLRRK I1915T on free eIF4E levels. eIF4E was precipitated using m^7GTP-sepharose from the brain tissues of flies with or without 5% H_2O_2 treatment for 24 h. eIF4E-bound (m^7GTP-bound) and free (unbound) 4E-BP were estimated. Graph shows the percentage of free 4E-BP in total 4E-BP after normalization with m^7GTP-bound eIF4E level. Values represent means ± s.d. from three experiments (*$P<0.05$; **$P<0.01$ versus GFP; 4E-BP WT in corresponding treatment).

or animal viability (Bernal and Kimbrell, 2000), suggesting that it is dispensable for cell growth or survival under normal conditions. However, *d4E-BP* mutant flies are defective in responses to various stress stimuli (Bernal and Kimbrell, 2000; Teleman *et al*, 2005; Tettweiler *et al*, 2005). d4E-BP has also been proposed to exert an effect as a metabolic brake for fat metabolism under stress conditions (Teleman *et al*, 2005). Whether this role of 4E-BP is relevant to dLRRK function in stress resistance and DA neuron maintenance remains to be tested. eIF4E, the target of 4E-BP, functions

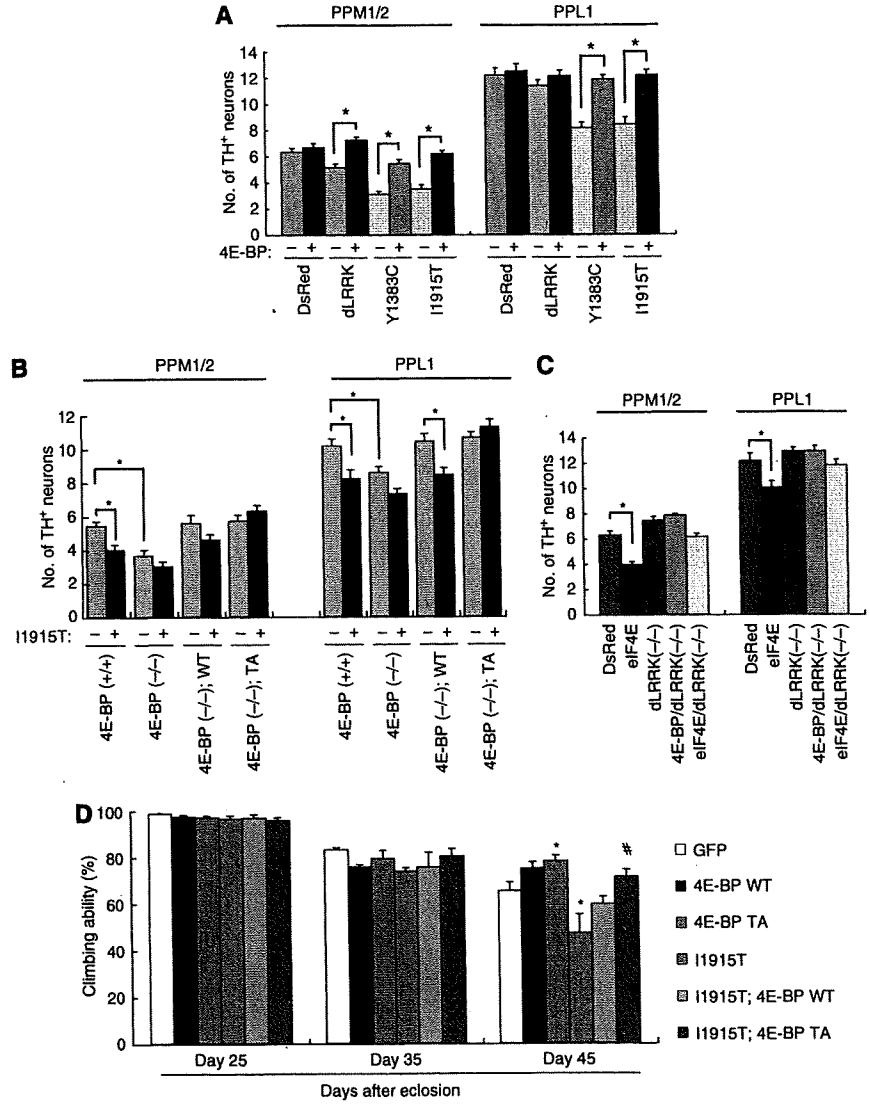

Figure 5 4E-BP overexpression suppresses dysfunction and degeneration of DA neuron induced by mutant dLRRK. (**A**) d4E-BP co-expression rescues dLRRK overexpression-induced DA neuron loss (*$P<0.01$ in Student's *t*-test, $n=12$). *TH-Gal4* was used to direct transgene expression and 60-day-old flies aged at 25 °C were analysed. (**B**) d4E-BP TA protects against DA neuron loss in dLRRK I1915T Tg flies. *TH-Gal4* was used to direct transgene expression and 30-day-old flies aged at 29 °C were analysed. *$P<0.05$, $n=14$. (**C**) *dLRRK* LOF rescues deIF4E overexpression-induced DA neuron loss (*$P<0.01$, $n=12$). *TH-Gal4* crosses were analysed as in (A). (**D**) Pan-neuronal expression of dLRRK I1915T under *elav-Gal4* control leads to gradual motor defect with age. The loss of climbing ability in dLRRK I1915T-expressing flies was rescued by 4E-BP TA expression. GFP serves as control. The values represent means ± s.d. from 20 trials ($n=30$; *$P<0.05$ versus GFP; #$P<0.01$ versus I1915T by one-way ANOVA with Bonferroni/Dunn test). The genotypes are as follows: *elav-Gal4>UAS-GFP* (GFP), *elav-Gal4>UAS-4E-BP WT* (4E-BP WT), *elav-Gal4>UAS-4E-BP TA* (4E-BP TA), *elav-Gal4>UAS-dLRRK I1915T* (I1915T), *elav-Gal4>UAS-dLRRK I1915T/UAS-4E-BP WT* (I1915T; 4E-BP WT), *elav-Gal4>UAS-dLRRK I1915T/UAS-4E-BP TA* (I1915T; 4E-BP TA). Male flies were used for the assay.

primarily in regulating general protein translation *in vitro*. It has been suggested that overactivation of eIF4E is linked to the aging process and lifespan regulation *in vivo* (Ruggero *et al*, 2004; Syntichaki *et al*, 2007). We observed that overexpression of eIF4E as well as dLRRK leads to an aging-related phenotype in DA neurons, which strongly suggested that chronic attenuation of 4E-BP activity promotes oxidative stress and consequent aging in DA neurons. This is consistent with the finding of similar patterns of gene expression under oxidative stress and aging conditions (Landis *et al*, 2004), and the fact that PD caused by LRRK2 mutations is of late onset, with aging being a major risk factor.

We analysed effects of removing dLRRK activity using a transposon insertion allele (*dLRRK*−), a chromosomal deletion allele (*dLRRK Df*) and gene knockdown (*dLRRK* RNAi). *dLRRK*(−/−), *dLRRK* (*Df*/−) and *dLRRK* RNAi flies are all resistant to oxidative stress treatments and show reduced endogenous ROS damages. In the paraquat treatment assay, *dLRRK* (*Df*/−) appeared more resistant than *dLRRK*(−/−) (Figure 2D). It is possible that *dLRRK*(−/−), which contains a transposon insertion in the COR domain of dLRRK, is not a null allele, although we have not been able to detect a truncated protein product using an antibody against the N-terminus of the protein. Alternatively, the chromosomal

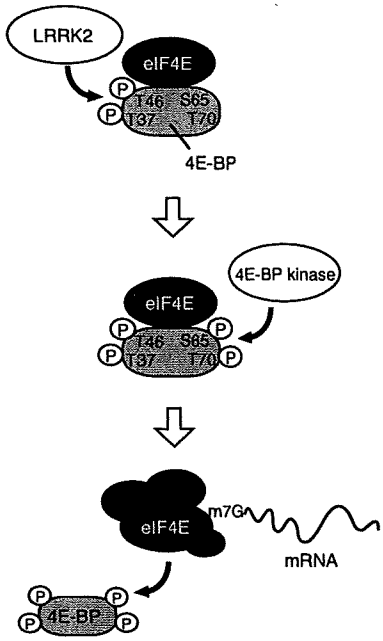

Figure 6 A model depicting 4E-BP phosphorylation by dLRRK. Phosphorylation of 4E-BP at T37/T46 residues by LRRK2 (upper) facilitates subsequent phosphorylation at T70 and S65 (middle). Hyperphosphorylated 4E-BP is released from mRNA cap-binding protein eIF4E, which leads to the formation of an initiation factor complex including eIF4E for protein translation (lower).

deletion in *dLRRK* (*Df*) may include other gene(s) relevant to stress sensitivity. One candidate is the gene for PI3K *Dp110* subunit. A recent study reported that *dLRRK*(−/−) animals are slightly sensitive to hydrogen peroxide but are comparable to control animals in response to paraquat (Wang *et al*, 2008). It is possible that the different genetic backgrounds and the nutrient conditions may account for the divergent results. In our studies, we backcrossed the mutant chromosome to w^- WT background for six generations in an effort to eliminate potential background mutations. A consistent finding from our study and two other studies of *dLRRK*(−/−) animals is that dLRRK is dispensable for the maintenance of DA neurons (Lee *et al*, 2007; Wang *et al*, 2008), although in one study it was reported that *dLRRK*(−/−) animals show reduced TH immunoreactivity and shrunken morphology of DA neurons (Lee *et al*, 2007). In contrast, overexpression of hLRRK2 containing a pathogenic G2019S mutation (Liu *et al*, 2008), or overexpression of mutant dLRRK as reported here, caused DA neuron degeneration, supporting the fact that the pathogenic mutations cause disease by a GOF mechanism.

The pathogenesis caused by mutations in LRRK2 could be partially explained by their higher kinase activity. Indeed, some pathogenic mutants of both hLRRK2 and dLRRK show elevated kinase activity towards 4E-BP. However, other mutants (e.g., hLRRK2 Y1699C and dLRRK Y1383C) did not show elevated kinase activity *in vivo*. Therefore, these pathogenic hLRRK2 mutations might confer cellular toxicity through mechanisms other than protein translation. For example, some hLRRK2 mutants are prone to aggregation in cultured cells (Smith *et al*, 2005; Greggio *et al*, 2006). Consistently, dLRRK Y1383C mutant appeared as more prominent vesicular aggregates in fly DA neurons (data not shown). Nevertheless, the facts that overexpression of eIF4E is sufficient to confer hypersensitivity to oxidative stress and DA neuron loss and that co-expression of 4E-BP suppresses the dopaminergic toxicity caused by more than one pathogenic dLRRK mutants provide compelling evidence that the eIF4E–4E-BP axis has an important function in mediating the pathogenic effects of overactivated LRRK2. The more downstream events that lead to DA neurotoxicity remain to be elucidated. So far, we have found no clear evidence of altered autophagy, caspase activation or DNA fragmentation (data not shown).

There are several possibilities of how elevated protein translation could contribute to PD pathogenesis. First, given that protein synthesis is a highly energy-demanding process, stimulation of protein translation by LRRK2 could perturb cellular energy and redox homoeostasis. This could be especially detrimental in aged cells or stressed post-mitotic cells such as DA neurons. Second, increased protein synthesis could lead to the accumulation of misfolded or aberrant proteins, overwhelming the already compromised ubiquitin proteasome and molecular chaperone systems in aged or stressed cells. Third, altered LRRK2 kinase activity may affect synapse structure and function, which is known to involve local protein synthesis. Deregulation of this process could lead to synaptic dysfunction and eventual neurodegeneration.

Materials and methods

Drosophila genetics
See Supplementary data for details.

RT–PCR, plasmids and siRNAs
See Supplementary data for details.

Cell culture, immunopurification, western blot analysis and m^{7}GTP pull-down assay
Transfection of 293T cell, immunopurification of FLAG-protein from the transfected cell lysate and western blot analysis were performed as described previously (Imai *et al*, 2000, 2001). For preparation of fly samples for western blot analysis, fly heads were directly homogenized in 20 μl of SDS sample buffer per head using a motor-driven pestle. After centrifugation at 16 000*g* for 10 min, the supernatant was used in SDS–PAGE. For immunoprecipitation or m^{7}GTP pull-down assay, fly heads were homogenized in 10 μl of lysis buffer per head (50 mM Tris, pH 7.4, 150 mM NaCl, 5 mM EDTA, 10% glycerol, 1% Triton X-100, 0.5 mM DTT, 60 mM β-glycerolphosphate, 1 mM sodium vanadate, 20 mM NaF and complete inhibitor cocktail (Roche)). After centrifugation at 16 000*g* for 30 min, the supernatant was subjected to the assays. For m^{7}GTP pull-down assay, the supernatant of each lysate from 15 fly heads was incubated with 15 μl of m^{7}GTP-Sepharose (GE Healthcare) for 2 h. The precipitates were washed four times with lysis buffer. The precipitates (m^{7}GTP-bound) and the flow through (unbound) were analysed by western blot. Densitometry was analysed using Image J software from the US National Institute of Health (http//rsb.info.nih.gov/ij/).

Antibodies
See Supplementary data for details of antibodies resources.

In vitro phosphorylation assay
FLAG–dLRRK or FLAG–hLRRK2 immunopurified from transfected 293T cells and mock fractions processed by the same procedures were used as kinase sources. Five micrograms of His–d4E-BP or His–h4E-BP1 were incubated with FLAG–dLRRK or FLAG–hLRRK2 in a kinase reaction buffer (20 mM HEPES, pH 7.4, 15 mM $MgCl_2$, 5 mM EGTA, 0.1% Triton X-100, 0.5 mM DTT, 1 mM β-glycerolpho-

sphate and 2.5 μCi [γ-^{32}P]-ATP) for 30 min at 30 °C. The reaction mixture was suspended in SDS sample buffer and then subjected to SDS–PAGE and autoradiography.

Dopamine measurement

Monoamine measurement was performed as described previously (Yang *et al*, 2005), with investigators blind to the genotypes during the measurement.

Whole-mount immunostaining

Counting of TH-positive neurons was performed by whole-mount immunostaining of brain samples as described previously (Yang *et al*, 2006). Immunohistochemical analysis for 4-HNE was carried out in whole-mount brain samples of animals originated from *TH-Gal4>UAS-GFP* crossed to the indicated genotypes. Anti-4HNE signals were normalized with GFP signals derived from the UAS-GFP transgene expressed in the same TH-positive neurons. Image J software was used for signal quantification. For dot blot analysis of 4-HNE, total lysates made from fly heads were spotted onto a PVDF membrane and subsequently incubated with anti-4HNE (1:15) overnight. As a control, we used western blot analysis of β-tubulin from the same extracts. Properties of the 4-HHE antibody are described on the manufacturer's Web site: http://www.jaica.com/biotech/e/. Immunohistochemical analyses were performed using a Carl Zeiss laser scanning microscope system.

Oxidative stress assay

The survival rate of 10-day-old male adult flies ($n=15$–20 per vial) kept in a vial containing a tissue paper socked with 0.5% H_2O_2 or 2 mM paraquat prepared in Schneider's insect medium was measured as described (Yang *et al*, 2005). To control for isogeny, *dLRRK*(−/−), *4E-BP*(−/−), *UAS-4E-BP* and the *Da-Gal4* driver were backcrossed to w^- background for six generations. For studies in transgenic overexpression, the *UAS-dLRRK* transgenes, *UAS-dLRRK RNAi* and *UAS-d4E-BP TA* transgenic lines were generated in w^- background and thus have a matched genetic background. For the analysis in Figures 4 and 5, *Thor*^{1} (*4E-BP null*) and its revertant served as 4E-BP(−/−) and 4E-BP(+/+), respectively. *UAS-d4E-BP WT* and *UAS-d4E-BP TA* transgenics, which shows similar protein expression of d4E-BP, were backcrossed to 4E-BP(−/−) background for five generations.

Climbing assay

The climbing assay was performed similarly to a previously described protocol (Feany and Bender, 2000). Thirty flies were placed in a plastic vial (18.6 cm in height × 3.5 cm^2 in area) and gently tapped to bring them down to the bottom of the vial. Flies were given 18 s to climb, and the number of flies above 6 cm from the bottom was counted. Twenty trials were performed for each time point for the same set of flies.

Statistical analysis

Two-way repeated-measures ANOVA was performed in multiple groups unless otherwise indicated. If positive ($P<0.05$), the means between the control and the specific groups were analysed using the Dunnett's test.

Supplementary data

Supplementary data are available at *The EMBO Journal* Online (http://www.embojournal.org).

Acknowledgements

We are grateful to Drs B Edgar, DA Kimbrell, P Lasko, D Pan, N Sonenberg, Z Zhang, T Xu and the *Drosophila* Stock centers for flies; Drs NJ Dyson, P Lasko, N Sonenberg and J Sierra, and RH Wharton for antibodies; Drs P Bitterman and V Polunovsky for plasmids; and Dr S Guo for reading the manuscripts. Special thanks go to J Quach, Y Zhang and W Lee for technical supports and members of the Lu lab for discussions. Supported by the NIH (R21 NS056878-01, R01 AR054926-01), the McKnight, Beckman and Sloan Foundations (BL), the Naito Foundation, JSPS Postdoctoral Fellowships for Research Abroad and Program for Young Researchers from Special Coordination Funds for Promoting Science and Technology commissioned by MEXT in Japan (YI).

References

Bernal A, Kimbrell DA (2000) *Drosophila* Thor participates in host immune defense and connects a translational regulator with innate immunity. *Proc Natl Acad Sci USA* **97:** 6019–6024

Fadden P, Haystead TA, Lawrence Jr JC (1997) Identification of phosphorylation sites in the translational regulator, PHAS-I, that are controlled by insulin and rapamycin in rat adipocytes. *J Biol Chem* **272:** 10240–10247

Feany MB, Bender WW (2000) A *Drosophila* model of Parkinson's disease. *Nature* **404:** 394–398

Gao X, Pan D (2001) TSC1 and TSC2 tumor suppressors antagonize insulin signaling in cell growth. *Genes Dev* **15:** 1383–1392

Gingras AC, Gygi SP, Raught B, Polakiewicz RD, Abraham RT, Hoekstra MF, Aebersold R, Sonenberg N (1999a) Regulation of 4E-BP1 phosphorylation: a novel two-step mechanism. *Genes Dev* **13:** 1422–1437

Gingras AC, Raught B, Gygi SP, Niedzwiecka A, Miron M, Burley SK, Polakiewicz RD, Wyslouch-Cieszynska A, Aebersold R, Sonenberg N (2001) Hierarchical phosphorylation of the translation inhibitor 4E-BP1. *Genes Dev* **15:** 2852–2864

Gingras AC, Raught B, Sonenberg N (1999b) eIF4 initiation factors: effectors of mRNA recruitment to ribosomes and regulators of translation. *Annu Rev Biochem* **68:** 913–963

Gloeckner CJ, Kinkl N, Schumacher A, Braun RJ, O'Neill E, Meitinger T, Kolch W, Prokisch H, Ueffing M (2006) The Parkinson disease causing LRRK2 mutation I2020T is associated with increased kinase activity. *Hum Mol Genet* **15:** 223–232

Greggio E, Jain S, Kingsbury A, Bandopadhyay R, Lewis P, Kaganovich A, van der Brug MP, Beilina A, Blackinton J, Thomas KJ, Ahmad R, Miller DW, Kesavapany S, Singleton A, Lees A, Harvey RJ, Harvey K, Cookson MR (2006) Kinase activity is required for the toxic effects of mutant LRRK2/dardarin. *Neurobiol Dis* **23:** 329–341

Heesom KJ, Avison MB, Diggle TA, Denton RM (1998) Insulin-stimulated kinase from rat fat cells that phosphorylates initiation factor 4E-binding protein 1 on the rapamycin-insensitive site (serine-111). *Biochem J* **336** (Part 1): 39–48

Holcik M, Sonenberg N (2005) Translational control in stress and apoptosis. *Nat Rev Mol Cell Biol* **6:** 318–327

Imai Y, Soda M, Inoue H, Hattori N, Mizuno Y, Takahashi R (2001) An unfolded putative transmembrane polypeptide, which can lead to endoplasmic reticulum stress, is a substrate of Parkin. *Cell* **105:** 891–902

Imai Y, Soda M, Takahashi R (2000) Parkin suppresses unfolded protein stress-induced cell death through its E3 ubiquitin-protein ligase activity. *J Biol Chem* **275:** 35661–35664

Inoki K, Corradetti MN, Guan KL (2005) Dysregulation of the TSC-mTOR pathway in human disease. *Nat Genet* **37:** 19–24

Jaleel M, Nichols RJ, Deak M, Campbell DG, Gillardon F, Knebel A, Alessi DR (2007) LRRK2 phosphorylates moesin at threonine-558: characterization of how Parkinson's disease mutants affect kinase activity. *Biochem J* **405:** 307–317

Jenner P (2003) Oxidative stress in Parkinson's disease. *Ann Neurol* **53** (Suppl 3): S26–S36; discussion S28–S36

Landis GN, Abdueva D, Skvortsov D, Yang J, Rabin BE, Carrick J, Tavare S, Tower J (2004) Similar gene expression patterns characterize aging and oxidative stress in Drosophila melanogaster. *Proc Natl Acad Sci USA* **101:** 7663–7668

Lee SB, Kim W, Lee S, Chung J (2007) Loss of LRRK2/PARK8 induces degeneration of dopaminergic neurons in *Drosophila*. *Biochem Biophys Res Commun* **358:** 534–539

Liu Z, Wang X, Yu Y, Li X, Wang T, Jiang H, Ren Q, Jiao Y, Sawa A, Moran T, Ross CA, Montell C, Smith WW (2008) A *Drosophila* model for LRRK2-linked parkinsonism. *Proc Natl Acad Sci USA* **105:** 2693–2698

Mata IF, Wedemeyer WJ, Farrer MJ, Taylor JP, Gallo KA (2006) LRRK2 in Parkinson's disease: protein domains and functional insights. *Trends Neurosci* **29:** 286–293

Miron M, Verdu J, Lachance PE, Birnbaum MJ, Lasko PF, Sonenberg N (2001) The translational inhibitor 4E-BP is an effector of PI(3)K/Akt signalling and cell growth in *Drosophila*. *Nat Cell Biol* **3:** 596–601

Moore DJ, West AB, Dawson VL, Dawson TM (2005) Molecular pathophysiology of Parkinson's disease. *Annu Rev Neurosci* **28:** 57–87

Nishimura I, Yang Y, Lu B (2004) PAR-1 kinase plays an initiator role in a temporally ordered phosphorylation process that confers tau toxicity in *Drosophila*. *Cell* **116:** 671–682

Paisan-Ruiz C, Jain S, Evans EW, Gilks WP, Simon J, van der Brug M, Lopez de Munain A, Aparicio S, Gil AM, Khan N, Johnson J, Martinez JR, Nicholl D, Carrera IM, Pena AS, de Silva R, Lees A, Marti-Masso JF, Perez-Tur J, Wood NW *et al* (2004) Cloning of the gene containing mutations that cause PARK8-linked Parkinson's disease. *Neuron* **44:** 595–600

Potter CJ, Huang H, Xu T (2001) *Drosophila* Tsc1 functions with Tsc2 to antagonize insulin signaling in regulating cell growth, cell proliferation, and organ size. *Cell* **105:** 357–368

Richter JD, Sonenberg N (2005) Regulation of cap-dependent translation by eIF4E inhibitory proteins. *Nature* **433:** 477–480

Ruggero D, Montanaro L, Ma L, Xu W, Londei P, Cordon-Cardo C, Pandolfi PP (2004) The translation factor eIF-4E promotes tumor formation and cooperates with c-Myc in lymphomagenesis. *Nat Med* **10:** 484–486

Saucedo LJ, Gao X, Chiarelli DA, Li L, Pan D, Edgar BA (2003) Rheb promotes cell growth as a component of the insulin/TOR signalling network. *Nat Cell Biol* **5:** 566–571

Smith WW, Pei Z, Jiang H, Moore DJ, Liang Y, West AB, Dawson VL, Dawson TM, Ross CA (2005) Leucine-rich repeat kinase 2 (LRRK2) interacts with parkin, and mutant LRRK2 induces neuronal degeneration. *Proc Natl Acad Sci USA* **102:** 18676–18681

Sonenberg N, Rupprecht KM, Hecht SM, Shatkin AJ (1979) Eukaryotic mRNA cap binding protein: purification by affinity chromatography on sepharose-coupled m^7GDP. *Proc Natl Acad Sci USA* **76:** 4345–4349

Syntichaki P, Troulinaki K, Tavernarakis N (2007) eIF4E function in somatic cells modulates ageing in *Caenorhabditis elegans*. *Nature* **445:** 922–926

Taylor JP, Mata IF, Farrer MJ (2006) LRRK2: a common pathway for parkinsonism, pathogenesis and prevention? *Trends Mol Med* **12:** 76–82

Teleman AA, Chen YW, Cohen SM (2005) 4E-BP functions as a metabolic brake used under stress conditions but not during normal growth. *Genes Dev* **19:** 1844–1848

Tettweiler G, Miron M, Jenkins M, Sonenberg N, Lasko PF (2005) Starvation and oxidative stress resistance in *Drosophila* are mediated through the eIF4E-binding protein, d4E-BP. *Genes Dev* **19:** 1840–1843

Wang D, Tang B, Zhao G, Pan Q, Xia K, Bodmer R, Zhang Z (2008) Dispensable role of *Drosophila* ortholog of LRRK2 kinase activity in survival of dopaminergic neurons. *Mol Neurodegener* **3:** 3

West AB, Moore DJ, Biskup S, Bugayenko A, Smith WW, Ross CA, Dawson VL, Dawson TM (2005) Parkinson's disease-associated mutations in leucine-rich repeat kinase 2 augment kinase activity. *Proc Natl Acad Sci USA* **102:** 16842–16847

Yamaguchi S, Ishihara H, Yamada T, Tamura A, Usui M, Tominaga R, Munakata Y, Satake C, Katagiri H, Tashiro F, Aburatani H, Tsukiyama-Kohara K, Miyazaki J, Sonenberg N, Oka Y (2008) ATF4-mediated induction of 4E-BP1 contributes to pancreatic beta cell survival under endoplasmic reticulum stress. *Cell Metab* **7:** 269–276

Yang Y, Gehrke S, Haque ME, Imai Y, Kosek J, Yang L, Beal MF, Nishimura I, Wakamatsu K, Ito S, Takahashi R, Lu B (2005) Inactivation of *Drosophila* DJ-1 leads to impairments of oxidative stress response and phosphatidylinositol 3-kinase/Akt signaling. *Proc Natl Acad Sci USA* **102:** 13670–13675

Yang Y, Gehrke S, Imai Y, Huang Z, Ouyang Y, Wang JW, Yang L, Beal MF, Vogel H, Lu B (2006) Mitochondrial pathology and muscle and dopaminergic neuron degeneration caused by inactivation of *Drosophila* Pink1 is rescued by Parkin. *Proc Natl Acad Sci USA* **103:** 10793–10798

Zimprich A, Biskup S, Leitner P, Lichtner P, Farrer M, Lincoln S, Kachergus J, Hulihan M, Uitti RJ, Calne DB, Stoessl AJ, Pfeiffer RF, Patenge N, Carbajal IC, Vieregge P, Asmus F, Muller-Myhsok B, Dickson DW, Meitinger T, Strom TM *et al* (2004) Mutations in LRRK2 cause autosomal-dominant parkinsonism with pleomorphic pathology. *Neuron* **44:** 601–607

Journal of Neurochemistry

JOURNAL OF NEUROCHEMISTRY | 2008 | 107 | 171–185 doi: 10.1111/j.1471-4159.2008.05607.x

Pael-R transgenic mice crossed with parkin deficient mice displayed progressive and selective catecholaminergic neuronal loss

Hua-Qin Wang,*,†,‡ Yuzuru Imai,§ Haruhisa Inoue,*,†,¶ Ayane Kataoka,† Sachiko Iita,† Nobuyuki Nukina† and Ryosuke Takahashi*,†,¶

*Department of Neurology, Kyoto University Graduate School of Medicine, Kyoto, Japan

†Brain Science Institute (BSI), RIKEN, Saitama, Japan

‡Department of Biochemistry and Molecular Biology, China Medical University, Shenyang, Liaoning, China

§Institute of Development, Aging and Cancer, Tohoku University, Miyagi, Japan

¶Core Research for Evolutional Science and Technology (CREST), Japan Science and Technology Corporation, Kawaguchi, Japan

Abstract

Parkin, a ubiquitin ligase, is responsible for autosomal recessive juvenile parkinsonism (AR-JP). We identified parkin-associated endothelin receptor-like receptor (Pael-R) as a substrate of parkin, whose accumulation is thought to induce unfolded protein response (UPR) -mediated cell death, leading to dopaminergic neurodegeneration. To create an animal model of AR-JP, we generated parkin knockout/Pael-R transgenic (*parkin*-ko/*Pael-R*-tg) mice. *parkin*-ko/*Pael-R*-tg mice exhibited early and progressive loss of dopaminergic as well as noradrenergic neurons without formation of inclusion bodies, recapitulating the pathological features of AR-JP. Evidence of activation of UPR and up-regulation of dopamine and its metabolites were observed throughout the lifetime. Moreover, complex I activity of mitochondria isolated from *parkin*-ko/*Pael-R*-tg mice was significantly reduced later in life. These findings suggest that persistent induction of unfolded protein stress underlies chronic progressive catecholaminergic neuronal death, and that dysfunction of mitochondrial complex I and oxidative stress might be involved in the progression of Parkinson's disease. *parkin*-ko/*Pael-R*-tg mice represents an AR-JP mouse model displaying chronic and selective loss of catecholaminergic neurons.

Keywords: dopaminergic neuron, endoplasmic reticulam stress, mitochondrial complex I, Pael-R, parkin.

J. Neurochem. (2008) **107**, 171–185.

Parkinson's disease (PD) is an age-related movement disorder including tremor, rigidity, bradykinesia and postural instability. A variety of evidence has strongly demonstrated that these motor symptoms are related to the selective degeneration of dopaminergic neurons in the substantia nigra pars compacta (SNpc) (Olanow and Tatton 1999). However, the underlying molecules and cellular pathways that mediate neuronal death remain poorly defined. Although the majority of PD cases appear to present without a family history of disease, several genes such as *α-synuclein, parkin, DJ-1, PINK-1,* and *LRRK2* have been identified as the genes responsible for familial PD. Among genes identified to date, mutations of parkin have been shown to be the cause of autosomal recessive juvenile parkinsonism (AR-JP) (Kitada *et al.* 1998; Lucking *et al.* 2000). Parkin functions as a protein-ubiquitin ligase (E3) and loss of E3 activity causes AR-JP, suggesting that substrate(s) of parkin, which cannot be properly degraded and accumulates in AR-JP patients, may cause dysfunction and eventually the death of susceptible neurons (Imai *et al.* 2000; Shimura *et al.* 2000; von Coelln *et al.* 2004a). In addition, increasing evidence suggests that partial loss of parkin E3 function resulting from S-nitrosylation or covalent modification by dopamine

Received March 6, 2008; revised manuscript received July 17, 2008; accepted July 18, 2008.

Address correspondence and reprint requests to Ryosuke Takahashi, M.D., Department of Neurology, Kyoto University Graduate School of Medicine, Shogoin, Sakyo-ku, Kyoto 606-8507, Japan.
E-mail: ryosuket@kuhp.kyoto-u.ac.jp

H.-Q.W. and Y.I. equally contributed to this work.

Abbreviations used: AR-JP, autosomal recessive juvenile parkinsonism; DOPAC, 3, 4-dihydroxyphenylacetic acid; ER, endoplasmic reticulum; HVA, homovanillic acid; LC, locus coeruleus; PD, Parkinson's disease; PDGF, platelet-derived growth factor; TH, tyrosine hydroxylase; UPR, unfolded protein response.

may also play a role in late-onset and sporadic PD (Chung *et al.* 2004; Yao *et al.* 2004; LaVoie *et al.* 2005). Parkin-associated endothelin receptor-like receptor (Pael-R/GPR37) was identified as an intracellular substrate of parkin, which has a propensity to accumulate in an unfolded form in the endoplasmic reticulum (ER) (Imai *et al.* 2001). When over-expressed in cultured cells, Pael-R tends to become misfolded and insoluble, inducing ER stress, and ultimately leading to cell death. Parkin ubiquitinates and promotes the degradation of misfolded species of Pael-R, resulting in the suppression of ER stress-induced cell death. The finding that panneuronal expression of Pael-R in *Drosophila* causes progressive selective loss of dopaminergic neurons further strongly supports a pathogenetic role for Pael-R in AR-JP (Yang *et al.* 2003). However, none of parkin null mouse models demonstrates either alteration in gross brain morphology or dopaminergic neuronal loss except for a recent report by Rodriguez-Navarro *et al.* (Goldberg *et al.* 2003; Itier *et al.* 2003; Von Coelln *et al.* 2004b; Perez and Palmiter 2005; Rodriguez-Navarro *et al.* 2007). A number of α-synuclein transgenic (tg), DJ-1- or PINK1- null mice models have also been created (Fernagut and Chesselet 2004; Goldberg *et al.* 2005; Kim *et al.* 2005). Although each of these models reproduces some of the pathological features of PD, obvious degeneration of dopaminergic neurons is not observed. The apparent preservation of dopaminergic neurons in these genetically modified animals suggests that obvious dopaminergic neuronal death may occur over a more protracted time scale than the average life spans of experimental animals, or that additional pathogenic event(s) may be required to induce such cell death.

Given that RNA interference (RNAi)-mediated down-regulation of endogenous *parkin* enhances the neurodegeneration of Pael-R tg *Drosophila* (Yang *et al.* 2003), deletion of the parkin gene in Pael-R tg mice may enhance the accumulation of Pael-R, resulting in neuronal degeneration. To test this hypothesis, we generated parkin-deficient/Pael-R-over-expressing double-mutant mice by crossbreeding parkin knockout (ko) mice with Pael-R tg mice. Here we show that *parkin*-ko/*Pael-R*-tg double-mutant mice exhibit early and progressive loss of dopaminergic neurons without formation of inclusion bodies, recapitulating the pathological characteristics of AR-JP. We provide compelling *in vivo* evidence of a mechanism linking progressive neuronal degeneration with persistent chronic ER stress. We also report that *parkin*-ko/*Pael-R*-tg double-mutant mice exhibit down-regulation of Ndufs4 and Ndufa10, two phosphorylated subunits of mitochondrial complex I, resulting in decrease in activity of mitochondrial complex I, suggesting that impairment of complex I activity might be the common pathway involved in various forms of PD including AR-JP. Moreover, the dopamine up-regulation caused by Pael-R over-expression seems to enhance oxidative stress, contributing to selective dopaminergic neuronal death.

Materials and methods

Generation of double-mutant mice over-expressing human Pael-R on a parkin null background

Transgenic mice that express human Pael-R under the control of the murine prion (PrP) or platelet-derived growth factor (PDGF) promoter (Imai *et al.* 2007) as well as the exon 3-deleted parkin null mice (Kitao *et al.* 2007) were produced as described. Double-mutant mice were generated by crossbreeding these two existing mouse lines. In the first step, parkin ko mice were bred to heterozygous Pael-R transgenic mice. Double-heterozygous mice generated in the first round of breeding were once more crossed with parkin ko mice to generate heterozygous Pael-R transgenic mice on a parkin null background (*parkin*-ko/non-tg or *parkin*-ko/*Pael-R*-het-tg). The *parkin*-ko/PrP- or PDGF-*Pael-R*-hetero-tg were cross-bred with each other to generate parkin null mice without Pael-R transgene (*parkin*-ko/*Pael-R*-non-tg), heterozygous or homozygous Pael-R transgenic mice lacking parkin (*parkin*-ko/PrP- or PDGF-*Pael-R*-het-tg and *parkin*-ko/PrP- or PDGF-*Pael-R*-homo-tg, respectively). In two successive breeding steps, cohorts of littermates with or without endogenous parkin expression and with or without transgenic Pael-R expression were generated in ratios consistent with Mendelian principles. Age-matched littermate mice were used in all experiments. All procedures involving animals conformed to the guidelines of the Institutional Animal Care Committee of RIKEN BSI and Kyoto University Graduate School of Medicine.

Immunohistochemistry

Mice were injected with pentobarbital (100 mg/kg; Sigma, St Louis, MO, USA) and perfused transcardially with ice-cold phosphate-buffered saline (PBS, pH 7.4), followed by 4% paraformaldehyde in PBS. Serial coronal sections at 16-μm thickness were collected on slides. Using standard avidin–biotin peroxidase method (Elite standard kit SK6100; Vector Laboratories, Burlingame, CA, USA), deparaffinized sections were stained with primary antibodies against tyrosine hydroxylase (TH, Chemicon, Temecula, CA, USA), α-synuclein (BD Transduction Laboratories, Lexington, KY, USA), BiP (Stressgen, Collegeville, PA, USA), CHOP (Santa Cruz Biotechnology, Santa Cruz, CA, USA) and ubiquitin (Dako, Carpinteria, CA, USA). For co-localization of TH with BiP or CHOP, deparaffinized sections were doubly stained with TH and BiP or CHOP, followed by reaction with Alexa 488- and 546-conjugated secondary antibodies (Molecular Probes, Eugene, OR, USA), and then examined with a LSM 510 confocal laser-scanning microscope (Carl Zeiss, Inc., Minneapolis, MN, USA).

Stereological analysis

Total numbers of TH-positive or Nissl-positive neurons in SNpc and locus coeruleus (LC) were determined using an unbiased optical fractionator method (Stereoinvestigator, MicroBrightField) as previously described (West 1993; Goldberg *et al.* 2003; Von Coelln *et al.* 2004b).

Behavioral tests

The mouse cohort for behavioral tests comprised 20 *parkin*-ko/*Pael-R*-non-tg mice, *parkin*-ko/PrP-*Pael-R*-het-tg mice and *parkin*-ko/PrP-*Pael-R*-homo-tg mice each. All tests were carried out by investigators blinded to the genotype of the animals being tested.

Western blot

Immunolabeling was performed using primary antibodies against α-synuclein (BD Transduction Laboratories), Pael-R (Imai *et al.* 2001), PKR-like ER-resident kinase (PERK, Santa Cruz), XBP1 (Santa Cruz), BiP (BD Transduction Laboratories), caspase-12 (Oncogene, Cambridge, MA, USA) JNK1/2 (Santa Cruz), phospho-JNK1/2 (Santa Cruz), CHOP (BioLegend, San Diego, CA, USA), TH (Chemicon), dopamine transporter (Chemicon), and vesicular monoamine transporter 2 (VMAT2, Chemicon), as well as horseradish peroxidase-conjugated secondary antibodies and ECL solutions (Amersham Pharmacia Biotech, Piscataway, NJ, USA). For densitometric analysis, images were scanned and densitometry was performed using the NIH IMAGE 1.4 software (Scion Corporation, Frederick, MD, USA).

RNA extraction and real-time PCR

Total RNA was isolated from freshly dissected midbrains using TRIzol Reagent (Invitrogen, Carlsbad, CA, USA) and first strand cDNA was synthesized from 2 μg of total RNA using Super-Script™ II Rnase H⁻ Reverse Transcriptase (Invitrogen) according to the manufacturer's instructions. Real-time PCR analysis was performed in triplicate on the ABI prism 7000 sequence detection system (Applied Biosystems, Foster City, CA, USA) using the SYBR Green PCR Master mix (Applied Biosystems). Results of real-time PCR were normalized against those for actin and plotted as ratio versus *parkin*-ko/*Pael-R*-non-tg.

Mitochondrial preparation and complex I, II–III, and IV activity assays

The mitochondrial complexes I, II–III, and IV activity assays were performed in triplicate on isolated mitochondria preparations as previously described (Hsu *et al.* 2005). The mitochondrial complexes and complex I subunits were detected using Total OXPHOS Complexes Detection Kit (MitoScience, Eugene, OR, USA), anti-8 kDa subunit monoclonal antibody (MitoScience), anti-18 kDa subunit monoclonal antibody (MitoScience) and anti-42 kDa subunit polyclonal antibody (Biocompare). Anti-COXIV monoclonal antibody (Molecular Probes) and anti-porin monoclonal antibody (Calbiochem, San Diego, CA, USA) were used as loading controls.

Measurement of catecholamines (HPLC)

To determine the concentration of catecholamines in striatal tissues by HPLC with electrochemical detection, male mice (n = 12 each) were decapitated, striata were dissected. The tissue was weighed and sonicated in 0.5 ml of ice-cold 0.1 M perchloric acid, to which 3, 4-dihydroxybenzylamine (DHBA) (Sigma) was added as the internal standard. DA and metabolites were detected with series coulometric detector (ESA, Inc., Chelmsford, MA, USA). Data were collected and processed on a CHROMELEON™ Chromatography Data Systems 6.40 (Dionex, Sunnyvale, CA, USA).

Protein carbonyl assay

Brain homogenate was assayed for protein carbonyls according to the manufacturer's instructions (OxyBlot™ Protein Oxidation Detection Kit, Chemicon).

Statistics

All values are presented as the mean ± SEM. Results were tested for significance using one-way ANOVA, followed by the Bonferoni *post hoc* test (SPSS 15.0 software). A significance level of $p < 0.05$ was used.

Results

Generation of *parkin*-ko/*Pael-R*-tg double-mutant mice

Transgenic mice over-expressing human Pael-R driven by murine PrP or PDGF promoter, designated PrP-*Pael-R* tg or PDGF-*Pael-R* tg mice, respectively, were generated as previously shown (Imai *et al.* 2007). PrP-*Pael-R* tg mice exhibited mild but significant loss of dopaminergic neurons (Fig. 1a). Neurodegeneration was not observed in PDGF-*Pael-R* tg mice even at the age of 2 years (Fig. 1b), probably due to relatively low expression level of Pael-R (Imai *et al.* 2007). Two lines of PrP- and PDGF-*Pael-R* tg mice were bred with parkin null mice (Kitao *et al.* 2007) to generate parkin null without Pael-R transgene (*parkin*-ko/*Pael-R*-non-tg), parkin null with Pael-R heterozygous tg (*parkin*-ko/PrP- or PDGF-*Pael-R*-het-tg) and Pael-R homozygous tg (*parkin*-ko/PrP- or PDGF-*Pael-R*-homo-tg) mice. We confirmed that 26-month-old *parkin*-ko mice did not display dopaminergic cell loss as compared with wild-type mice (Fig. 1c). Pael-R tended to be more insoluble in the midbrain region (Fig. S1), and throughout life the steady-state levels of both endogenous Pael-R and over-expressed human Pael-R remained unchanged (data not shown). Although parkin deletion had no effect on endogenous Pael-R monomer levels, both Triton X-100 soluble and insoluble fractions of over-expressed Pael-R monomer were significantly increased in *parkin*-ko/PrP-*Pael-R*-het-tg mice compared with PrP-*Pael-R*-het-tg mice with wild-type (wt) parkin (Fig. 1d and e). A higher molecular-weight band corresponding to the size of Pael-R dimer was constantly observed in all the samples (Fig. 1d). The high-molecular-weight bands were also observed in Pael-R null mice, indicating that they at least partially represent non-specific signals (Fig. 1f). However, given that non-specific signals are assumed to be almost identical between Pael-R null and wild-type mice, the decreased signal intensity in higher molecular-weight bands in Pael-R null mice compared with wt mice indicates that the higher molecular-weight bands in Pael-R expressing mice comprise both Pael-R dimer and the non-specific signals, and the former species are increased in the Triton X-100 insoluble fraction of parkin null mouse brains (Fig. 1d–f). Taken together, these data in Fig. 1(e) suggest that although less prominent than Pael-R transgene, insoluble species of endogenous Pael-R aggregates are likely to be increased in parkin null mice from 6 months of age.

Age-related neurodegeneration of dopaminergic neurons in *parkin*-ko/*Pael-R*-tg double-mutant mice

Progressive catecholaminergic neuronal loss was observed in both PrP-*Pael-R* and PGDF-*Pael-R* tg mice crossed with parkin null mice.

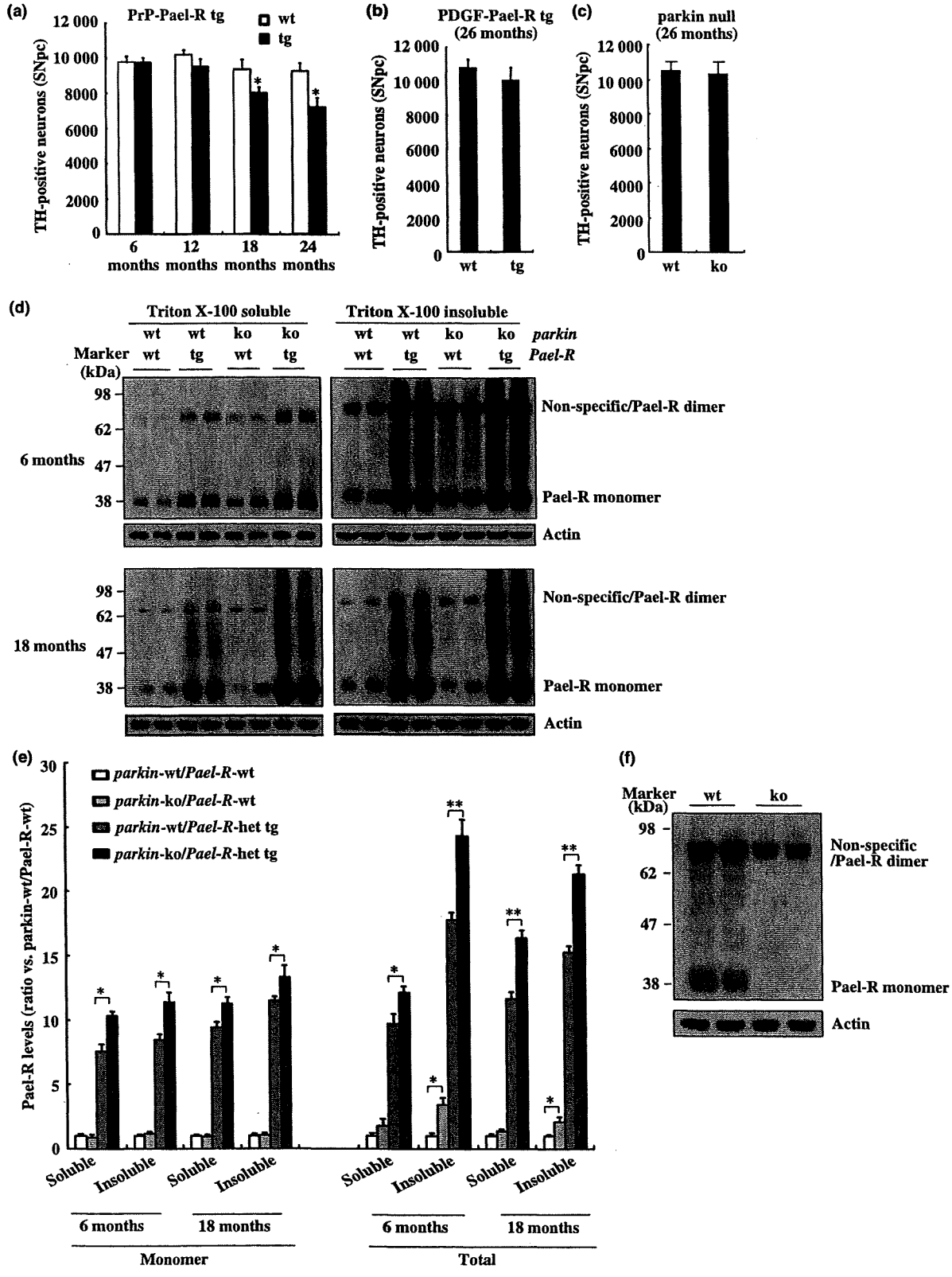

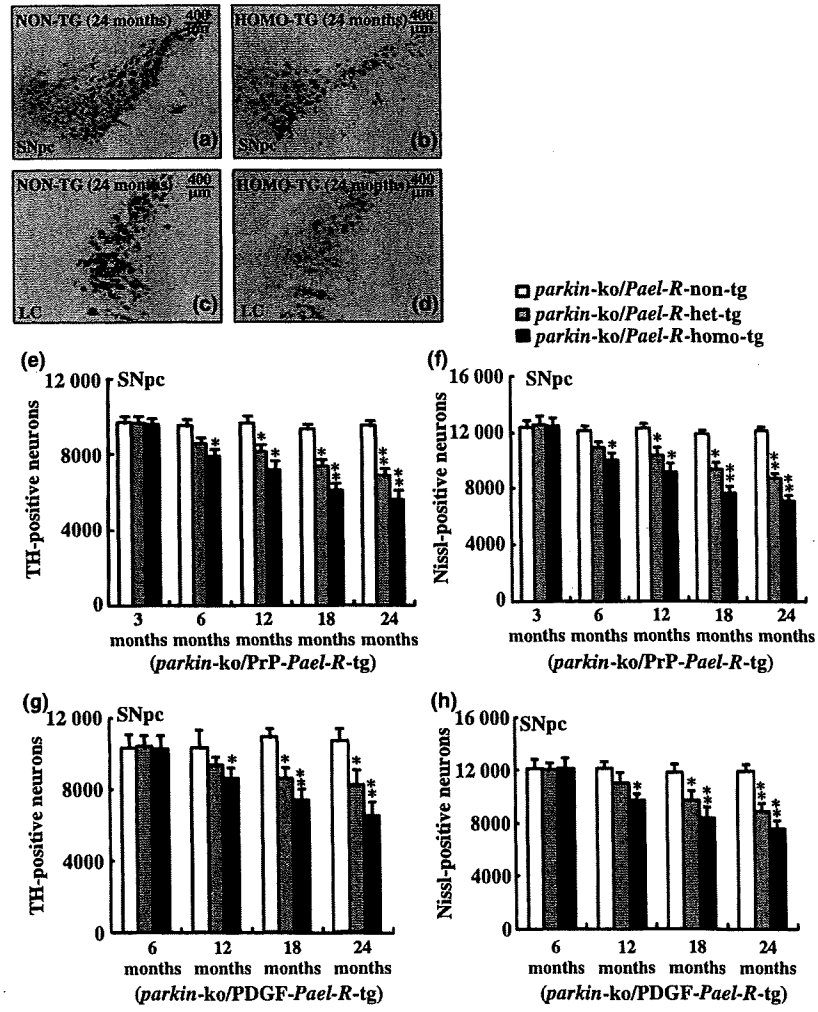

Fig. 2 Degeneration of TH-positive neurons in *parkin*-ko/PrP-*Pael-R*-tg double-mutant mice. (a and b) Representative photomicrographs of TH-immunoreactivity in SNpc of 24 months *parkin*-ko/*Pael-R*-non-tg and *parkin*-ko/PrP-*Pael-R*-homo-tg mice, respectively. (c and d) Representative photomicrographs of TH-immunoreactivity in LC of 24 months *parkin*-ko/*Pael-R*-non-tg and *parkin*-ko/PrP-*Pael-R*-homo-tg mice, respectively. (e and f), Number of TH-positive (e) or Nissl-positive neurons (f) in SNpc of *parkin*-ko/PrP-*Pael-R*-tg double-mutant mice. (g and h), Number of TH-positive (g) or Nissl-positive neurons (h) in SNpc of *parkin*-ko/PDGF-*Pael-R*-tg double-mutant mice. Data are expressed as mean ± SEM ($n = 10$). *, $p < 0.05$, **, $p < 0.01$ versus *parkin*-ko/*Pael-R*-non-tg.

Parkin-ko/PrP-*Pael-R*-tg mice exhibited decreased number of TH-positive neurons in the substantia nigra pars compacta (SNpc) and locus ceruleus (LC) regions compared with *parkin*-ko/*Pael-R*-non-tg mice (Fig. 2a–d). Unbiased stereological analyses revealed no difference in the number of TH-positive neurons in the SNpc of 3-month-old mice as assessed by either TH or Nissl staining. However, the number of TH-positive neurons exhibited age-dependent reduction beginning as early as 6 months in the *parkin*-ko/PrP-*Pael-R*-homo-tg double-mutant mice (Fig. 2e). The finding of similar loss of Nissl-positive neurons confirmed that the decrease of TH-positive neurons did not result from reduction of TH immunoreactivity, but from the loss of neurons *per se* (Fig. 2f). Similar loss of TH-positive neurons in the ventral tegmental area (VTA) and LC regions was also observed (Fig. S2a and b). Obvious loss of TH-positive

Fig. 1 Age-dependent loss of TH-positive neurons in Pael-R tg mice and absence of parkin increases steady-state levels of Pael-R. (a) Number of TH-positive neurons in Pael-R tg mice driven by PrP promoter. Values are the mean ± SEM ($n = 10$). *, $p < 0.05$, versus wild-type. (b) Number of TH-positive neurons in Pael-R tg mice driven by PDGF promoter ($n = 6$). (c) Number of TH-positive neurons in parkin ko mice ($n = 9$). (d) Representative western blot analysis of Triton X-100 soluble and insoluble lysates from midbrain of 6- and 18-month-old mice was performed using antibody recognizing both mouse and human Pael-R. The molecular weight was noted on the left. An antibody against actin was used as a loading control. (e) The expression levels of Pael-R (monomer, the band at approximately 38 kDa; total, the bands including Pael-R monomer, non-specific/Pael-R dimer, as well as smeared bands between Pael-R monomer and dimer) were quantified using optical density and normalized to that of actin. The protein levels are relative to those of parkin wt/Pael-R non-tg defined as 1. The data are presented as the mean ± SEM ($n = 6$). *, $p < 0.05$; **, $p < 0.01$. (f) Western blot analysis was performed on brain lysates from wt or Pael-R ko mice. The molecular weight was noted on the left.

neurons was observed at 18 months and 12 months in the PrP-Pael-R tg mice with and without parkin, respectively, indicating that loss of parkin predated the onset of neurodegeneration. The enhancement of Pael-R toxicity by parkin deficiency was more prominent in Pael-R tg mice driven by PDGF. Loss of TH-positive neurons became evident at 18 months of age in *parkin*-ko/PDGF-*Pael-R*-het-tg mice (Fig. 2g and h); whereas no frank neurodegeneration was observed in PDGF-*Pael-R*-het-tg mice expressing endogenous parkin even at 2 years of age (Fig. 1b). The number of hippocampal neurons in the dentate gyrus region, which also expressed high levels of Pael-R transgene (Fig. S1), was unaltered in *parkin*-ko/PrP-*Pael-R*-tg double-mutant mice (Fig. S3), suggesting that the cell loss occurred in catecholaminergic neuron-specific manner. Since *parkin*-ko/PrP-*Pael-R*-tg demonstrated more robust phenotype, we mainly analyzed *parkin*-ko/PrP-*Pael-R*-tg mice in the following analyses.

Tyrosine hydroxylase optical density in the striatum was also reduced in *parkin*-ko/PrP-*Pael-R*-homo-tg mice (Fig. 3a–c). This reduction in TH protein levels was confirmed by western blot at 18- and 24-month-old double-

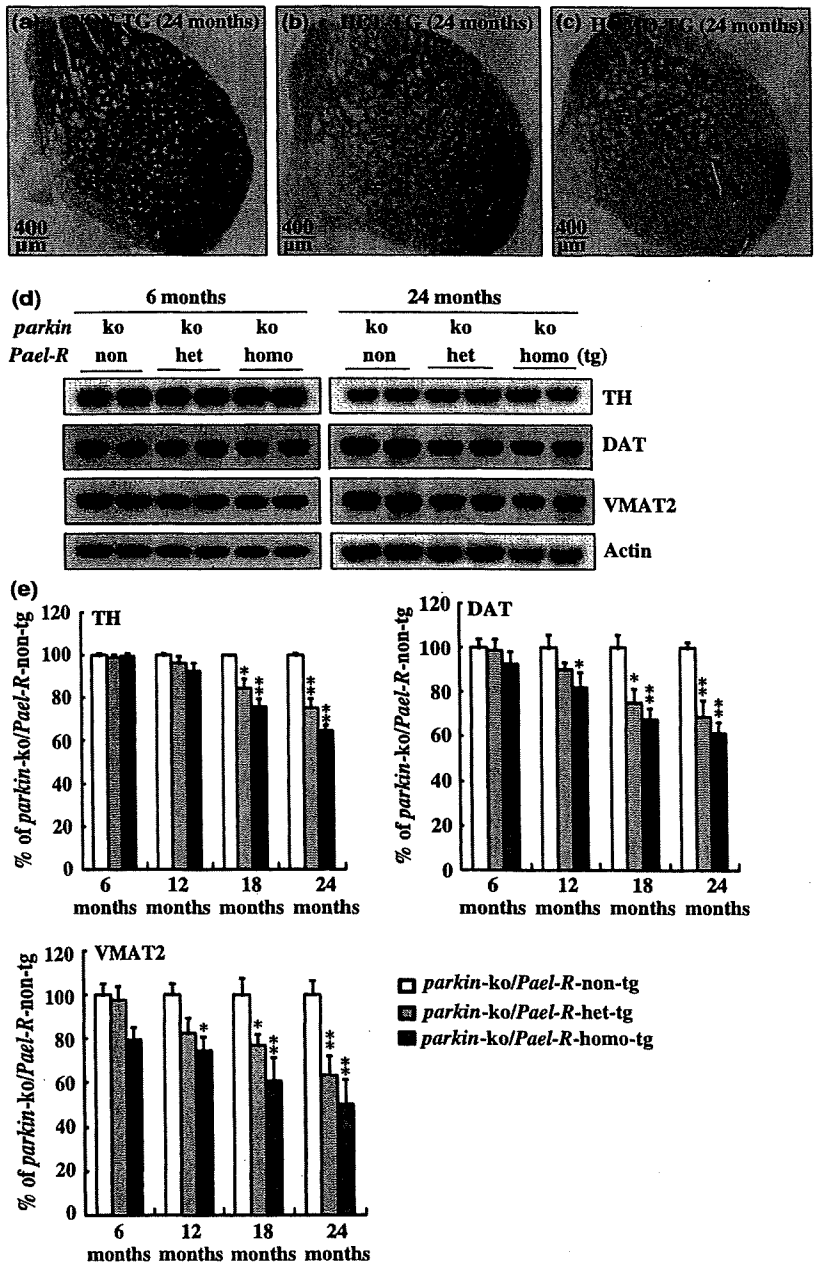

Fig. 3 Reduced TH-immunoreactivity in the striatum of *parkin*-ko/PrP-*Pael-R*-tg double-mutant mice. (a–c) Representative images of TH-immunoreactivity in the striatum of 24 months *parkin*-ko/*Pael-R*-non-tg, *parkin*-ko/PrP-*Pael-R*-het-tg and *parkin*-ko/PrP-*Pael-R*-homo-tg of mice, respectively. (d) Representative western blot images of TH, DAT and VMAT2 in young (6 M) and aged (24 M) mouse striatum. Actin was used as a loading control. (e) The expression levels of TH, DAT and VMAT2 (normalized to actin) were quantified using optical density. Data are expressed as mean ± SEM ($n = 6$). *, $p < 0.05$, **, $p < 0.01$ versus *parkin*-ko/*Pael-R*-non-tg.